Available online at www.sciencedirect.com
ScienceDirect
Earth and Planetary Science Letters 252 (2006) 223–244
EPSL
www.elsevier.com/locate/epsl

Hf isotope evidence for selective mobility of high-field-strength elements in a subduction setting: South Sandwich Islands

T.L. Barry [a,*], J.A. Pearce [b], P.T. Leat [c], I.L. Millar [d], A.P. le Roex [e]

[a] Cardiff University-BAS/NIGL, NIGL, BGS, Keyworth, Nottingham, NG12 5GG, UK
[b] Cardiff University, School of Earth, Ocean and Planetary Science, Main Building, Park Place, Cardiff, CF10 3YE, UK
[c] British Antarctic Survey (BAS), High Cross, Madingley Road, Cambridge, CB3 0ET, UK
[d] BAS/NIGL, BGS, Keyworth, Nottingham, NG12 5GG, UK
[e] Department of Geology, University of Cape Town, Rondebosch, 7700 South Africa

Received 12 August 2005; received in revised form 4 July 2006; accepted 18 September 2006
Available online 15 November 2006
Editor: V. Courtillot

Abstract

$^{176}Hf/^{177}Hf$ isotopes provide information about the behaviour of so-called immobile elements in subduction environments. Early studies of Hf isotopes in subduction zones reached different conclusions regarding the mobility of high-field-strength elements during subduction-related processes. To test the behaviour of Hf during subduction, we have examined the young, intra-oceanic South Sandwich subduction system. Combined $^{176}Hf/^{177}Hf$ and trace element ratios reveal that Hf may behave as both immobile and mobile, depending upon the exact spatial relationship of the arc volcano to the slab. Throughout most of the arc, magmas show no detectable Hf transfer from the slab to the wedge, perhaps because enrichment of the wedge took place by Hf-deficient, fluid-dominated processes. On the basis of $\Delta\varepsilon Nd$ values, which describe the Nd isotope deviation from a local MORB-OIB array, we can discern that northern volcanoes of the arc require a source enriched by fluids that originated from the oceanic crust, whereas southern arc volcanoes have a source modified by a higher proportion of sediment-derived fluids. However, close to the southern slab edge and in rear-arc settings, arc magmas were derived from a source that had undergone Hf addition; we attribute this to element transfer via partial melts from sediment. This implies that Hf mobility from the slab is possible where temperatures are sufficiently high to induce sediment melting rather than fluid generation alone. The implication of this work, for the majority of the arc, is that sediment-derived fluids contribute to magmatism and that sediment-derived melt does not.

Keywords: subduction; geochemistry; slab ends; hafnium isotopes; slab recycling; fluids

1. Introduction

The idea that mobile and immobile elements show contrasting behaviour during subduction is entrenched in the literature. Mobile, or non-conservative, elements are readily mobilized by fluids that move from the slab into the overlying mantle wedge, and become enriched in volcanic arc magmas derived by melting of that mantle. Conversely, immobile, or conservative, elements remain in the slab, and are therefore not enriched in the mantle wedge or in subsequent arc magmas (e.g. [1–6]). However, it is perhaps more meaningful to regard elements as mobile or immobile according to

* Corresponding author. Now at: Volcano Dynamics Group, CEPSAR, Open University, Walton Hall, Milton Keynes, MK7 6AA, UK. Tel.: +44 1908 653739; fax: +44 1908 655151.
E-mail address: T.L.Barry@open.ac.uk (T.L. Barry).

0012-821X/$ - see front matter © 2006 Elsevier B.V. All rights reserved.
doi:10.1016/j.epsl.2006.09.034

particular prevailing temperature and pressure conditions. Thus, subduction is not so much a matter of whether or not crustal material is recycled, but rather *where* it is recycled, *how* and by *how much*.

Transfer to the sub-arc mantle wedge of a particular element from subducting oceanic crust and/or its sedimentary cover (together constituting the 'slab') is understood to take place either (1) in aqueous fluids driven off the slab during dehydration reactions, or (2) in silicate melts generated by partial melting of subducted sediments, or (3) when there is a continuum between both processes [7–12]. The near-ubiquitous enrichment of volcanic arc magmas in the mobile elements such as Li, B, Rb, K, Ba, U and Pb [1–3,13,14]–elements that have high experimentally determined fluid/rock distribution coefficients [8,15–17]–indicate that enrichment by transfer in fluids is widespread beneath arcs. Surprisingly, elements that are not particularly soluble in aqueous fluids, such as Th and the light rare earth elements (REE), can also be enriched in arc magmas, indicating that such elements are also readily transferred to the sub-arc mantle wedge. Consequently, workers have proposed that element transfer by silicate melts, as well as aqueous fluids, must also play a common role in mantle wedge enrichment [6–8]. However, modelling calculations do not support slab melting as a common feature of all present-day subduction zones, as the temperature of the mantle is too low to melt relatively old and cold oceanic crust [18]. Moreover, between the extremes of low temperature aqueous fluids and high temperature melts is a spectrum of conditions which could cause elemental mobilization within which the role of supercritical fluids in subduction-related recycling is presently poorly understood [19].

Most isotopic tracers used in studies of subduction zones are isotopes of elements (Sr, Pb, Li, B, U) thought to be soluble in aqueous fluids (e.g. [20,21]). Conversely, Hf, like other high-field-strength elements (HFSE; Zr, Ti, Nb, Ta) and heavy rare-earth elements, is thought to behave 'conservatively' during subduction, on the basis that most arc basalts are not enriched in Hf relative to oceanic basalts. However, the assumption that Hf remains immobile during subduction processes has been questioned since the early studies of Hf isotopes from arc rocks [22]. Subsequent studies [23,24] drew little consensus, and only recently have ideas converged on the notion that Hf addition within arc rocks is possible, though under restricted conditions [25–27].

To further explore the behaviour of Hf during subduction we have chosen to examine the <15 My old intra-oceanic South Sandwich subduction system. Leat et al. [28] have already discovered, using trace element ratios and Sr–Nd isotopes, that sediment melt, rather than aqueous fluid, influences the mantle wedge chemistry beneath a slab-edge-proximal seamount and in back-arc spreading segments close to the slab-edge. They interpreted this finding as enhanced generation of subduction fluxes along the southern slab edge caused by influx of hot mantle. In this paper, we examine the role of sediment melt versus aqueous fluid in the enrichment of the mantle wedge by assessing the behaviour of Hf, and by inference other HFSE, in this subduction zone. We find that Hf mobility, implying sediment melt contribution, took place at the southern slab edge and also beneath rear-arc volcanoes whereas, elsewhere along the arc, element transfer is fluid-facilitated. In the north the fluid is derived dominantly from ocean crust but, in the south, requires a greater contribution from sediment.

2. Geological background

The South Sandwich arc in the southernmost Atlantic Ocean lies some 2000 km west of the Bouvet hotspot (Fig. 1) which underlies the triple junction between the mid-Atlantic ridge, the Southwest Indian Ridge (SWIR) and the South American-Antarctic Ridge (SAAR). The arc is entirely intra-oceanic, far-removed from any continental crust and, on the basis of magnetic anomalies, is situated on ~10 m.y. old oceanic crust of the Sandwich Plate [29,30] (Fig. 1). The Sandwich and South American plates converge at a rate between 70 and 79 mm/yr [31]. A transform discontinuity at 58°S separates older subducting South American lithosphere (ca. 80 Ma) to the north from younger lithosphere to the south (ca. 27 Ma); the crust in the north is ca. 400 m thick comprising siliceous and calcareous sediments whereas the younger crust in the south is a ca. 200 m thick siliceous-only sediment [32]. There is no evidence for accretion of sediment in the forearc [33], indicating that all the sediment arriving at the trench is subducted. Fault plane solutions provide evidence that the slab is in extension in the north but in compression in the south [34], and this likely reflects the relative ease of subduction of the colder slab in the north compared to a younger, warmer slab in the south. Slab dip is between 45° and 55° towards the west and, at depth, steepens slightly more in the north than the south (R.A. Livermore, pers. comm.). The northern edge of the slab is a tear in the South American plate, whereas the southern edge is the plate boundary between the South American and Antarctic plates (Fig. 1).

The arc comprises nine large, <3 Ma, volcanic islands (each covering over 2 km^2) plus a number of smaller islands and three prominent seamounts (Fig. 1). The arc crust has a maximum thickness of 20 km [30]. Arc rock

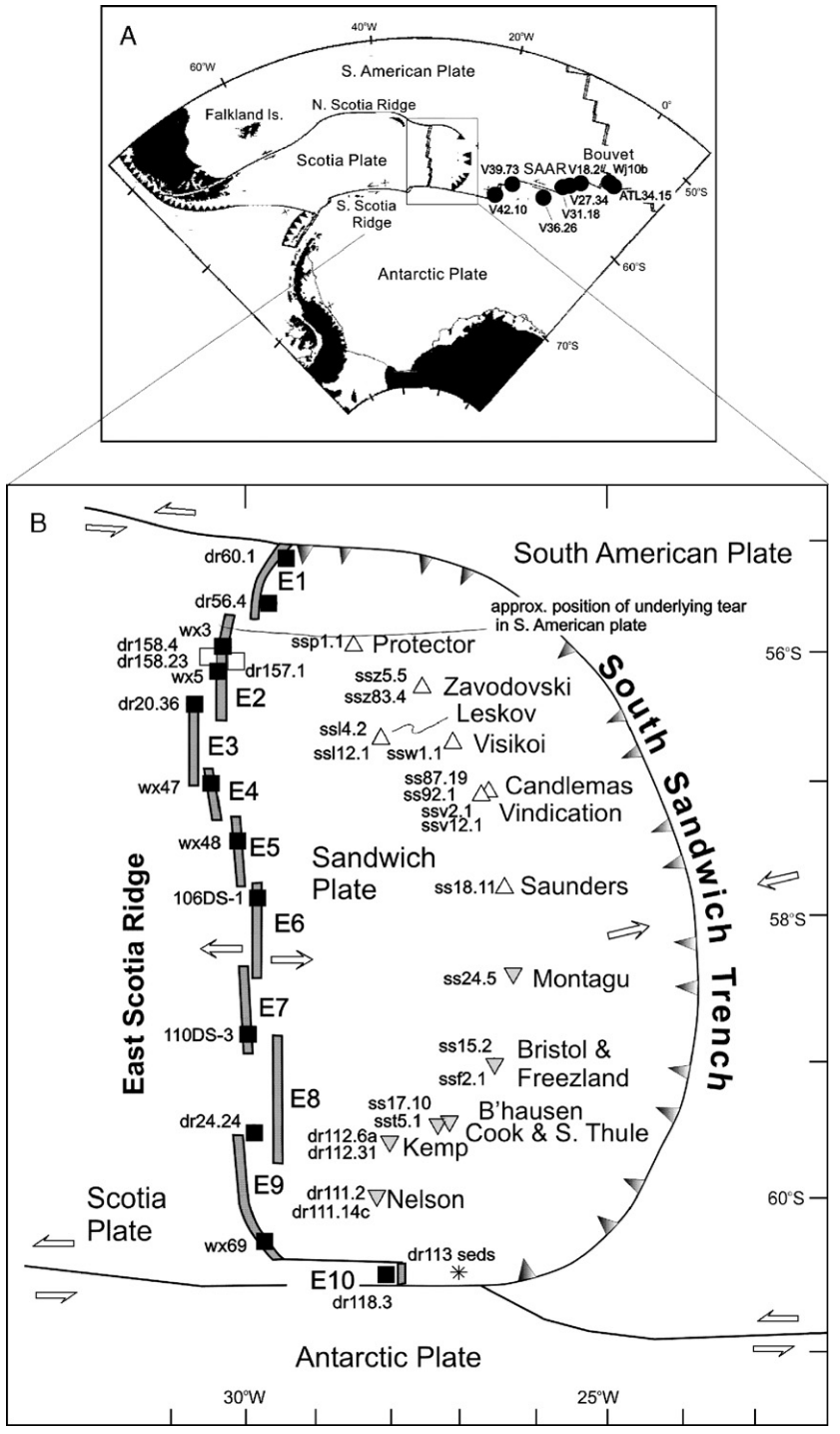

Fig. 1. Map of South Atlantic/Scotia Sea showing sample locations from Bouvet Island and along the SAAR (A) and within the arc–back-arc system (B). Symbols for sample localities, also for geochemical plots throughout the paper, are: solid circle—SAAR, solid square—MORB-like ESR, white square—subduction-modified ESR, white triangle—northern SSI arc, inverted grey triangle—southern SSI arc, star—pelagic sediment.

compositions vary from basaltic to rhyolitic and from low-K tholeiite, through tholeiitic to calc-alkaline [4,35]. There are no documented progressive compositional changes along the arc (e.g. [4]). Two of the volcanic islands are in rear-arc positions relative to the main trend of the arc; Leskov is the furthest set back from the arc by

Table 1a
New and published geochemical analyses for selected samples from the South Sandwich Arc, East Scotia Ridge, nearby sediments and the South American-Antarctic Ridge

	South Sandwich Island Arc (north to south)															
Location	Protector	Zavodovski	Zavodovski	Leskov	Leskov	Visikoi	Candlemas	Candlemas	Vindication	Vindication	Saunders	Montague	Bristol	Freezland	Bellingshausen	S. Thule
Sample no.	ssp1.1	ssz5.5	ssz83.4	ssl4.2	ssl12.1	ssw1.1	ss87.19	ss92.1	ssv2.1	ssv12.1	ss18.11	ss24.5	ss15.2	ssf2.1[1]	ss17.10	sst5.1[1]
Latitude (S)	55°45′	56°18′	56°18′	56°4′	56°4′	56°42′	57°05′	57°05′	57°1′	57°1′	57°45	58°25′	59°02′	59°02.5′	59°26′	59°28′
Rb	*12.0*	*4.7*	*6.3*	*19.6*	*18.7*	*6.8*	2.8	2.5	*1.8*	*1.5*	9.6	2.3	7.9	*16.2*	11.9	*17.0*
Sr	*114*	*139*	*140*	*208*	*197*	*137*	123	124	*112*	*112*	130	112	160	*196*	131	*159*
Y	*31.8*	*18.3*	*20.8*	*27.1*	*24.8*	*21.4*	14.5	10.6	*12.4*	*12.4*	20.2	10.7	21.5	*27.3*	28.5	*32.7*
Zr	*82.7*	*30.0*	*39.7*	*89.2*	*81.5*	*46.8*	23.1	17.4	*23.9*	*17.9*	45.8	15.2	48.8	*80.2*	73.4	*85.7*
Nb	*0.99*	*0.41*	*0.53*	*2.28*	*1.96*	*0.66*	0.26	0.26	*0.25*	*0.25*	0.70	0.17	0.75	*1.72*	1.11	*2.09*
Cs	*0.58*	*0.23*	*0.48*	*0.70*	*0.68*	*0.13*	0.13	0.10	*0.10*	*0.02*	0.48	0.09	0.30	*0.55*	0.52	*0.50*
Ba	*126*	*53*	*62*	*186*	*180*	*68*	35	97	*25*	*29*	77	25	86	*164*	118	*162*
La	*3.66*	*1.61*	*1.97*	*6.58*	*6.19*	*2.73*	1.00	0.72	*1.09*	*0.76*	2.43	0.70	2.62	*5.35*	3.92	*6.06*
Ce	*10.83*	*4.99*	*5.89*	*16.09*	*14.88*	*7.85*	3.27	2.37	*3.26*	*2.56*	7.09	2.24	7.73	*14.42*	11.04	*16.16*
Pr	*1.77*	*0.84*	*0.97*	*2.22*	*2.17*	*1.25*	0.60	0.43	*0.59*	*0.45*	1.13	0.39	1.27	*2.06*	1.76	*2.40*
Nd	*8.67*	*4.38*	*5.45*	*11.22*	*10.53*	*6.69*	3.48	2.36	*3.44*	*2.55*	5.99	2.35	6.75	*10.15*	9.29	*11.58*
Sm	*2.85*	*1.57*	*1.96*	*3.03*	*2.78*	*2.02*	1.27	0.93	*1.25*	*0.92*	2.00	0.89	2.20	*2.91*	2.95	*3.25*
Eu	*0.83*	*0.69*	*0.90*	*0.97*	*0.95*	*0.79*	0.56	0.44	*0.48*	*0.45*	0.73	0.39	0.79	*0.99*	0.96	*1.13*
Gd	*3.63*	*2.18*	*2.59*	*3.70*	*3.15*	*2.77*	1.90	1.30	*1.72*	*1.35*	2.70	1.32	2.95	*3.43*	3.84	*4.34*
Tb	*0.64*	*0.41*	*0.48*	*0.65*	*0.60*	*0.54*	0.35	0.24	*0.30*	*0.29*	0.49	0.24	0.53	*0.64*	0.68	*0.84*
Dy	*4.47*	*2.74*	*3.17*	*4.07*	*3.88*	*3.41*	2.23	1.67	*2.11*	*1.78*	3.16	1.69	3.37	*3.80*	4.46	*5.20*
Ho	*1.04*	*0.59*	*0.68*	*0.92*	*0.89*	*0.76*	0.50	0.37	*0.47*	*0.38*	0.70	0.37	0.73	*0.81*	0.98	*1.08*
Er	*2.96*	*1.84*	*2.00*	*2.75*	*2.48*	*2.35*	1.40	1.09	*1.39*	*1.17*	2.02	1.06	2.06	*2.48*	2.77	*3.40*
Tm	*0.50*	*0.28*	*0.32*	*0.45*	*0.43*	*0.35*	0.24	0.18	*0.22*	*0.21*	0.31	0.17	0.35	*0.42*	0.44	*0.50*
Yb	*3.32*	*1.83*	*2.09*	*3.00*	*2.72*	*2.18*	1.47	1.16	*1.44*	*1.18*	2.03	1.08	2.12	*2.76*	2.88	*3.42*
Lu	*0.50*	*0.29*	*0.30*	*0.45*	*0.40*	*0.33*	0.25	0.19	*0.23*	*0.19*	0.32	0.17	0.36	*0.41*	0.44	*0.52*
Hf	*2.29*	*0.86*	*1.26*	*2.50*	*2.25*	*1.44*	0.72	0.57	*0.90*	*0.54*	1.37	0.50	1.43	*2.12*	2.19	*2.67*
Ta	*0.08*	*0.02*	*0.03*	*0.12*	*0.13*	*0.07*	0.03	0.02	*0.03*	*0.02*	0.07	0.03	0.06	*0.11*	0.10	*0.16*
Pb	*3.22*	*1.40*	*2.18*	*2.51*	*2.66*	*2.01*	0.68	0.92	*0.77*	*0.77*	2.03	2.01	2.28	*3.25*	2.88	*4.26*
Th	*0.74*	*0.22*	*0.35*	*1.43*	*1.68*	*0.41*	0.13	0.10	*0.15*	*0.05*	0.44	0.09	0.48	*1.26*	0.85	*1.34*
U	*0.26*	*0.09*	*0.12*	*0.36*	*0.43*	*0.12*	0.05	0.06	*0.04*	*0.04*	0.15	0.04	0.15	*0.35*	0.28	*0.42*
$^{143}Nd/^{144}Nd$	*0.513069*[1]	*0.513084*[1]	0.513013	*0.512989*[1]	0.512934	*0.513052*[1]	0.513038	0.513035	*0.513073*[1]	*0.513014*[1]	0.512985	0.513062	0.513033	*0.513041*[1]	0.513027	*0.512982*[1]
εNd	8.41	8.70	7.32	6.85	5.78	8.08	7.81	7.74	8.49	7.33	6.78	8.28	7.70	7.86	7.60	6.71
ΔεNd	1.00	0.73	1.78	0.61	1.66	1.03	1.57	1.20	0.82	1.79	2.52	2.19	2.52	0.82	2.65	2.86
ΔNd	0.04	0.37	0.19	0.13	0.17	0.23	0.33	0.22	0.08	0.33	0.17	0.32	0.23	0.21	0.11	0.12
$^{176}Hf/^{177}Hf$	0.283149	0.283150	0.283137	0.283075	0.283074	0.283138	0.283148	0.283131	0.283145	0.283138	0.283145	0.283190	0.283180	0.283121	0.283181	0.283155
εHf	13.33	13.37	12.91	10.70	10.68	12.93	13.29	12.71	13.20	12.95	13.19	14.77	14.43	12.35	14.46	13.55
ΔHf	0.05	−0.31	−0.09	−0.02	−0.05	−0.12	−0.25	−0.12	0.01	−0.26	−0.06	−0.24	−0.12	−0.09	0.00	−0.01
$^{87}Sr/^{86}Sr$	*0.70394*[1]	*0.70402*[1]	0.70395	*0.70366*[1]	0.70365	*0.70372*[1]	0.70400	0.70401	*0.70385*[1]	0.70399	0.70408	0.70387	0.70380	*0.70379*[1]	0.70397	*0.70384*[1]
$^{206}Pb/^{204}Pb$	–	18.464	18.466	*18.513*[1]	18.482	18.628	18.831	18.254	*18.600*[1]	–	18.617	18.595	18.566	18.451	18.613	18.575
$^{207}Pb/^{204}Pb$	–	15.612	15.613	*15.567*[1]	15.580	15.629	15.621	15.611	*15.580*[1]	–	15.623	15.616	15.613	15.607	15.618	15.613
$^{208}Pb/^{204}Pb$	–	38.421	38.426	*38.415*[1]	38.395	38.607	38.551	38.264	*38.430*[1]	–	38.581	38.544	38.512	38.375	38.570	38.530

Previously published values written in italic. References denoted by superscript numbers are: (1) [4]; (2) [35]; (3) [28]; (4) [37]; (5) [41]; (6) [39]. East Scotia Ridge sample numbers in bold refer to those included in the regional Bouvet-SAAR-ESR array (see text). Note: Nd isotope ratios are all standardized to an accepted value for La Jolla value of $^{143}Nd/^{144}Nd=0.511860$, so it may appear different from originally published values.

Table 1a (*continued*)

	South Sandwich Island Arc (north to south)						South Atlantic sediment			East Scotia Ridge		East Scotia Ridge (north to south)				
Location	Cook	Nelson Smt	Nelson Smt	Kemp Smt	Kemp Smt	Kemp Smt	Sediment	Sediment	Sediment	E1	E1	E2	E2	E2	E2	E2
Sample no.	ss14.11[2]	dr111.2	dr111.14c	dr112.6a	dr112.11a1	dr112.31	dr113.3	dr113.7a	dr113.30	dr56.4	**dr60.1**	**wx3**	dr157.1	dr158.4	dr158.23	wx5
Latitude (S)	59°28′	60°0′	60°0′	59°55′	59°55′	59°55′	60°5′	60°5′	60°5′	55°32′	55°09′	56°6.01′	56°6.83′	56°6.93′	56°6.93′	56°8.16′
Rb	*4.7*	40.3	34.6	6.5	5.1	5.1	62.5	27.7	53.9	4.4	2.4	*9.4*	*15.9*	*24.3*	*15.0*	*14.3*
Sr	*165*	158	157	197	167	156	137	191	135	151	88	*230*	*296*	*378*	*240*	*238*
Y	*16.5*	31.0	25.8	12.6	13.9	14.3	18.1	29.5	19.1	16.0	15.1	*34.8*	*24.0*	*24.1*	*39.4*	*35.9*
Zr	*34.4*	112.1	98.1	24.5	29.1	26.4	76.8	175.7	76.2	50.9	34.8	*126.4*	*125.0*	*78.6*	*146.6*	*126.0*
Nb	*0.66*	4.36	3.88	0.43	0.57	0.52	5.29	10.14	4.42	3.86	0.78	*9.45*	*24.73*	*4.20*	*11.84*	*8.46*
Cs	*0.14*	–	–	–	–	–	2.81	0.90	2.43	0.06	0.11	*0.15*	*0.16*	*0.74*	*0.27*	*0.26*
Ba	*63*	312	226	63	100	91	775	356	600	53	20	*133*	*196*	*283*	*197*	*199*
La	*2.12*	11.30	9.84	2.07	2.19	2.00	14.69	13.11	14.06	3.02	1.31	*9.78*	*16.15*	*9.41*	*11.75*	*9.46*
Ce	*6.08*	25.20	22.50	5.51	6.15	5.51	31.27	30.33	30.13	7.38	3.77	*25.95*	*34.74*	*23.28*	*28.42*	*23.70*
Pr	*0.95*	3.34	2.92	0.81	0.95	0.89	3.71	4.22	3.64	1.12	0.69	*3.29*	*4.33*	*3.03*	*3.93*	*3.41*
Nd	*4.90*	14.59	12.80	4.12	5.01	4.65	15.06	19.08	14.94	5.55	3.95	*14.76*	*18.07*	*13.72*	*18.51*	*15.61*
Sm	*1.62*	3.68	3.20	1.39	1.56	1.53	3.21	4.77	3.25	1.67	1.42	*4.21*	*4.14*	*3.71*	*5.13*	*4.51*
Eu	*0.63*	0.94	0.83	0.52	0.56	0.56	0.84	1.44	0.83	0.64	0.56	*1.61*	*1.38*	*1.25*	*1.70*	*1.53*
Gd	*2.10*	4.01	3.52	1.73	1.79	1.75	3.00	4.91	3.17	2.02	1.82	*4.79*	*4.43*	*4.07*	*5.83*	*5.08*
Tb	*0.39*	0.75	0.64	0.31	0.35	0.36	0.50	0.87	0.52	0.38	0.37	*0.85*	*0.68*	*0.66*	*1.02*	*0.88*
Dy	*2.53*	4.82	4.12	1.99	2.33	2.33	2.95	5.24	3.11	2.44	2.35	*5.66*	*4.21*	*4.09*	*6.51*	*5.87*
Ho	*0.55*	1.03	0.89	0.43	0.50	0.51	0.61	1.07	0.65	0.52	0.51	*1.18*	*0.83*	*0.83*	*1.36*	*1.23*
Er	*1.63*	3.04	2.59	1.25	1.44	1.48	1.76	3.03	1.87	1.50	1.51	*3.36*	*2.31*	*2.35*	*3.87*	*3.51*
Tm	*0.25*	0.51	0.43	0.19	0.24	0.24	0.28	0.47	0.30	0.23	0.22	*0.52*	*0.35*	*0.37*	*0.61*	*0.54*
Yb	*1.64*	3.13	2.68	1.27	1.48	1.52	1.84	2.96	1.92	1.49	1.50	*3.37*	*2.17*	*2.31*	*3.79*	*3.52*
Lu	*0.26*	0.50	0.43	0.21	0.23	0.24	0.29	0.45	0.30	0.23	0.23	*0.53*	*0.34*	*0.36*	*0.59*	*0.55*
Hf	*1.04*	3.14	2.75	0.78	0.87	0.85	2.11	3.93	2.10	1.29	1.03	*3.09*	*2.96*	*2.03*	*3.63*	*3.22*
Ta	*0.05*	0.32	0.28	0.04	0.03	0.03	0.39	0.73	0.34	0.23	0.06	*0.55*	*1.52*	*0.27*	*0.70*	*0.53*
Pb	*0.93*	8.85	3.67	0.94	4.70	4.20	8.99	33.01	7.53	0.52	0.79	*1.60*	*3.07*	*2.64*	*1.88*	*1.93*
Th	*0.39*	4.36	3.62	0.47	0.44	0.40	4.86	2.35	4.51	0.40	0.15	*1.12*	*1.87*	*1.89*	*1.37*	*1.14*
U	*0.12*	1.20	1.04	0.15	0.14	0.14	1.36	0.64	1.13	0.12	0.05	*0.30*	*0.55*	*0.48*	*0.39*	*0.32*
$^{143}Nd/^{144}Nd$	*0.513027*[2]	*0.512673*[3]	*0.512690*[3]	*0.512980*[3]	–	0.513012	0.512426	0.512784	0.512469	0.513007	*0.513049*[3]	0.513014[4]	*0.512975*[4]	*0.512877*[4]	*0.512981*[4]	*0.512992*[4]
εNd	7.59	0.68	1.02	6.68	–	7.30	−4.13	2.86	−3.30	7.20	8.02	7.33	6.57	4.66	6.69	6.91
ΔεNd	2.29	3.31	2.93	3.22	–	1.90	1.96	1.94	2.48	1.24	0.43	0.55	2.55	3.10	1.02	1.17
ΔNd	0.25	0.11	0.10	0.34	–	0.38	0.39	0.06	0.40	0.09	0.05	0.16	0.25	0.41	0.20	0.17
$^{176}Hf/^{177}Hf$	0.283167	0.282942	0.282941	0.283168	0.283161	0.283141	0.282707	0.282973	0.282758	0.283112	0.283113	0.283091	0.283138	0.283086	0.283084	0.283098
εHf	13.97	6.01	5.96	14.00	13.76	13.05	−2.30	7.11	−0.48	12.02	12.04	11.28	12.95	11.12	11.04	11.53
ΔHf	−0.14	0.01	0.02	−0.25	−0.34	−0.31	−0.29	0.06	−0.30	0.02	0.04	−0.04	−0.09	−0.34	−0.07	−0.05
$^{87}Sr/^{86}Sr$	*0.70378*[2]	*0.70484*[3]	*0.70486*[3]	*0.70370*[3]	0.70373	0.70376	0.71166	0.70509	0.70946	0.70317	*0.70454*[3]	0.70320[4]	*0.70344*[4]	–	–	*0.70326*[4]
$^{206}Pb/^{204}Pb$	*18.574*[2]	*18.725*[3]	*18.719*[3]	*18.418*[3]	–	–	18.686	18.709	18.797	18.370	*18.564*[3]	18.359[4]	*19.316*[4]	*18.455*[4]	*18.328*[4]	*18.324*[4]
$^{207}Pb/^{204}Pb$	*15.598*[2]	*15.621*[3]	*15.637*[3]	*15.580*[3]	–	–	15.640	15.633	15.648	15.553	*15.603*[3]	15.594[4]	*15.587*[4]	*15.570*[4]	*15.549*[4]	*15.542*[4]
$^{208}Pb/^{204}Pb$	*38.479*[2]	*38.628*[3]	*38.658*[3]	*38.293*[3]	–	–	38.667	38.656	38.749	38.177	*38.421*[3]	38.293[4]	*38.930*[4]	*38.370*[4]	*38.161*[4]	*38.145*[4]

(*continued on next page*)

Table 1a (*continued*)

	East Scotia Ridge (north to south)								Bouvet and SAAR (east to west)							
Location	E3	E4	E5	E6	E7	E8	E9	E10	SWIR	Bouvet Is.	SAAR	SAAR	SAAR	SAAR	SAAR	SAAR
Sample no.	**dr20.36**	wx47	**wx48**	**106 DS-1**	**110DS-3**	dr24.24	**wx69**	dr118.3	ATL34.15	WJ10b	v18.2	v27.34	v31.18	v36.26	v39.73	v42.10
Latitude (S)	56°24′	57°02′	57°25′	57°49′	58°44′	59°28′	60°20′	60°35′			55°51.9′	56°53.7′	57°34.4′	58°08.8′	58°39.1′	59°21.8′
Rb	4.5	11.7	0.7	1.3	3.8	5.4	6.2	6.5	19.1	62.0	11.2	8.5	3.8	14.9	8.0	2.2
Sr	196	237	145	99	96	167	189	222	306	304	147	331	151	179	214	158
Y	26.6	28.2	26.2	31.2	28.6	21.8	27.6	30.2	46.4	74.4	48.0	29.5	34.8	49.9	29.6	47.4
Zr	99.5	109.9	96.5	92.5	95.2	65.1	128.1	99.6	247.4	677.4	153.2	138.5	114.2	198.3	115.5	187.6
Nb	4.80	4.43	2.06	1.94	3.92	1.45	6.04	5.33	28.26	86.19	4.83	13.58	5.22	7.36	7.30	4.30
Cs	–	0.22	0.01	0.00	0.03	–	0.10	–	0.16	0.65	0.45	0.09	0.09	0.78	0.30	0.01
Ba	36	143	9	11	30	67	65	70	208	582	30	144	32	33	52	15
La	4.52	5.98	2.94	3.23	4.37	3.00	6.23	6.08	25.54	66.04	5.95	11.59	5.22	8.87	6.77	6.95
Ce	12.42	15.54	9.32	10.47	12.37	8.70	15.74	16.13	55.90	130.80	17.38	26.84	14.16	24.27	16.86	20.74
Pr	1.92	2.42	1.69	1.94	2.10	1.39	2.49	2.55	7.48	17.03	3.00	3.84	2.34	3.98	2.56	3.47
Nd	10.03	12.05	8.97	10.45	10.74	7.24	12.05	12.44	32.79	69.36	15.87	17.75	12.16	20.22	12.54	17.67
Sm	2.97	3.70	3.12	3.76	3.62	2.31	3.73	3.77	8.07	14.74	5.17	4.47	3.89	5.92	3.67	5.36
Eu	1.07	1.29	1.18	1.30	1.22	0.84	1.32	1.35	2.53	4.29	1.74	1.54	1.41	1.92	1.34	1.78
Gd	3.67	4.55	4.05	5.04	4.78	2.89	4.54	4.21	8.75	14.27	6.60	4.92	4.92	7.12	4.33	6.49
Tb	0.68	0.80	0.73	0.92	0.87	0.53	0.81	0.80	1.39	2.24	1.20	0.81	0.89	1.26	0.75	1.16
Dy	4.29	5.18	4.79	6.28	5.90	3.45	5.20	5.07	8.05	12.55	7.64	4.90	5.63	7.78	4.63	7.30
Ho	0.91	1.11	1.02	1.30	1.23	0.75	1.09	1.05	1.61	2.50	1.64	1.01	1.18	1.64	0.96	1.55
Er	2.62	3.14	2.85	3.66	3.48	2.19	3.06	2.95	4.47	7.08	4.80	2.90	3.47	4.84	2.80	4.58
Tm	0.39	0.46	0.42	0.54	0.52	0.36	0.44	0.48	0.65	1.06	0.73	0.42	0.51	0.72	0.41	0.68
Yb	2.52	3.03	2.74	3.65	3.46	2.11	2.90	2.86	4.02	6.60	4.63	2.72	3.28	4.62	2.65	4.39
Lu	0.39	0.45	0.40	0.53	0.50	0.33	0.43	0.44	0.62	1.02	0.72	0.42	0.51	0.72	0.41	0.69
Hf	2.58	2.92	2.53	3.14	3.16	1.79	3.10	2.42	6.79	16.17	4.17	3.43	3.02	4.85	2.76	4.52
Ta	0.33	0.29	0.15	0.13	0.23	0.10	0.35	0.35	1.86	5.47	0.33	0.90	0.33	0.49	0.46	0.29
Pb	0.98	1.12	0.47	0.46	0.59	1.60	0.79	0.63	1.65	4.79	0.80	9.44	0.42	0.80	15.06	17.63
Th	0.37	0.65	0.11	0.13	0.26	0.38	0.45	0.64	2.37	7.58	0.35	0.82	0.34	0.49	0.47	0.27
U	0.20	0.19	0.05	0.05	0.09	0.12	0.15	0.20	0.73	2.41	0.16	0.34	0.15	0.28	0.20	0.12
$^{143}Nd/^{144}Nd$	*0.513084*[5]	*0.513018*[6]	*0.513135*[6]	*0.513143*[6]	*0.513095*[6]	0.513082	*0.513030*[6]	*0.513036*[5]	0.512898	0.512842	0.513077	0.512915	–	–	0.512980	0.513064
εNd	8.70	7.41	9.69	9.85	8.91	8.66	7.65	7.76	5.07	3.99	8.56	5.41	–	–	6.68	8.31
ΔεNd	0.41	1.13	0.16	0.10	0.33	1.55	0.06	1.62	0.07	0.29	0.82	1.45	–	–	0.95	0.60
ΔNd	−0.07	0.01	−0.14	0.08	0.04	0.03	−0.09	0.24	−0.03	−0.31	−0.05	0.13	–	–	0.07	−0.07
$^{176}Hf/^{177}Hf$	0.283138	0.283116	0.283166	0.283170	0.283143	0.283180	0.283084	0.283148	0.282986	0.282953	0.283148	0.283052	0.283133	0.283138	0.283081	0.283130
εHf	12.94	12.17	13.93	14.07	13.12	14.42	11.03	13.30	7.57	6.40	13.30	9.90	12.77	12.94	10.93	12.66
ΔHf	0.14	0.08	0.17	0.18	0.19	0.06	0.15	−0.11	0.13	0.28	0.11	0.01	0.09	0.10	0.04	0.13
$^{87}Sr/^{86}Sr$	*0.70285*[5]	*0.70329*[6]	*0.70251*[6]	*0.70262*[6]	*0.70283*[6]	0.70307	*0.70310*[6]	*0.70325*[5]	0.70335	0.70368	0.70323	0.70345	0.70279	0.70314	0.70314	0.70272
$^{206}Pb/^{204}Pb$	*18.115*[5]	*18.255*[6]	*18.025*[6]	*17.832*[6]	*17.885*[6]	18.360	*17.935*[6]	*18.211*[5]	19.140	19.534	–	18.747	–	–	18.684	18.673
$^{207}Pb/^{204}Pb$	*15.493*[5]	*15.530*[6]	*15.495*[6]	*15.463*[6]	*15.473*[6]	15.554	*15.513*[6]	*15.551*[5]	15.820	15.654	–	15.767	–	–	15.668	15.663
$^{208}Pb/^{204}Pb$	*37.733*[5]	*38.051*[6]	*37.571*[6]	*37.399*[6]	*37.506*[6]	38.174	*37.659*[6]	*37.874*[5]	39.463	39.156	–	38.569	–	–	38.208	38.189

a distance of ca. 50 km, and Freezland is slightly offset behind Bristol Island. The seamounts included in this study are all situated near the slab edges, Protector in the north, and Kemp and Nelson in the south (Fig. 1).

The back-arc spreading centre of the East Scotia Ridge (ESR) has been active for at least 15 My [30] and lies approximately 200 km to the west of the South Sandwich arc (Fig. 1). It comprises ten segments from E1 in the north to E10 in the south. The ridge is spreading at a full rate of 62 to 71 mm/yr [31,36]. E1 is propagating north into the South Sandwich trench and overlies downwarped South American Plate rather than subducted slab, a consequence of a tear in the South American Plate (Fig. 1). Segments E3 – 8, in the central region of the spreading centre, have rift-like median valley morphologies indicative of intermediate rates of magma production. In contrast, E2 and E9 have axial highs similar to those of fast spreading ridges. Segments E2 and E9 are shallower (ca. 2600 m) than the other segments (>4000 m in segments E5 and E6) [36]. The higher rate of magmatism in segments E2 and E9 may result from increased mantle flow around the slab edges that enables replenishment of their source regions with fertile mantle from the enriched Bouvet domain, as well as from additional mantle flux resulting from proximity to the downgoing slab [28,36–38]. Segment E2 shows a wide range of compositions varying from MORB-like (e.g. WX.3 [39]) to arc-like (e.g. DR.157.1). Although a small number of samples indicate a pronounced subduction-derived component (e.g. DR.158.4 [37]), in general, subduction input to the back-arc magmatism is small [37,39]. Segment E10 is very poorly defined and is offset trenchward from the main ridge axis (Fig. 1). It lies very close to the southern slab edge, at the plate boundary between the South American Plate and the South Sandwich Plate, and is closer to the trench than Nelson seamount, which forms the most southerly part of the arc.

3. Sample selection and analytical techniques

Samples for this study were selected from each of the South Sandwich Islands and seamounts (Fig. 1; Tables 1a and b). In addition to the arc samples, we selected representative samples from each segment of the back-arc East Scotia Ridge (Fig. 1). We also selected for analysis a small number of sediment samples in order to constrain likely compositions of downgoing sediment into the South Sandwich subduction zone. The samples are from Site 118 (Fig. 1; 60.5°S, 27.0°W, from depths 2200 to 1910 m b.s.l. at the eastern end of a scarp). Seismic surveys across this site indicate a 1 to 2 km thick sediment cover overlying basement [40]. For completeness, we have included three samples in the data table. Samples DR.113.3 and DR.113.30 are diatomaceous oozes, whereas sample DR.113.7a is largely volcaniclastic.

We used eight samples from the nearby South American-Antarctic mid-ocean ridge (SAAR) system to define the local OIB-MORB array. These are from Bouvet Island (WJ10b), from a segment east of the island along the Southwest Indian Ridge (SWIR) (ATL34.15), and from each of the major ridge segments along the SAAR between the Bouvet triple junction and the trench (see Fig. 1 for localities; Tables 1a and b).

On the selected representative suite of samples, we undertook new geochemical analyses, including Hf–Sr–Nd–Pb isotopes. Whole rock samples were prepared for analysis by crushing in an agate grinding container (tema mill). Major, trace and REE data, as well as Sr, Nd, and Pb isotopes, for many of the selected samples have been presented elsewhere [4,28,35] but, where such data did not exist, new trace and REE data were analysed by X-series Thermoelemental ICP-MS at Cardiff University following the procedure of Pearce et al. [4]. Accuracy and precision information for the runs are given in Appendix 1.

Isotopic analyses were undertaken at the NERC Isotope Geosciences Laboratory (NIGL), UK. All samples were prepared unleached. Determinations of Sr, Nd and Pb isotopes followed the procedures of [42,43]. Sr and Nd were run as the metal species on single Ta and double Re–Ta, respectively, using Finnigan MAT 262 and Triton multi-collector mass spectrometers. Sr and Nd were run in static mode. The effects of fractionation during runs were eliminated by normalizing Sr isotopes to a value for $^{86}Sr/^{88}Sr$ of 0.1194 and $^{143}Nd/^{144}Nd$ to a value of $^{146}Nd/^{144}Nd$ of 0.7219. Sample values for $^{87}Sr/^{86}Sr$ and $^{143}Nd/^{144}Nd$ are reported relative to accepted values of NBS 987 (0.71024) and J&M value of 0.511125 that cross calibrates to an accepted value of 0.51186 for La Jolla, respectively. Minimum uncertainties are derived from external precision of standard measurements that over the course of the analysis average 0.710242± 0.000014 (2σ, $n=21$) for $^{87}Sr/^{86}Sr$ and 0.511186± 0.000007 (2σ, $n=13$) for J&M $^{143}Nd/^{144}Nd$.

Pb isotopes were analysed on a VG Axiom MC-ICP-MS, with mass fractionation corrected within-run using a Tl-doping method [44]. We used a $^{203}Tl/^{205}Tl$ value of 0.41876, which was determined empirically by cross-calibration with NBS 981. All Pb isotope ratios have been corrected relative to the NBS 981 composition of [45]. The blank contribution was less than 100 pg.

Procedures for Hf isotope preparation follow those described by Kempton et al. [46] and were run on MC-ICP-MS machines, VG P54 at NIGL and Finnigan Neptune at Frankfurt Goethe University. The data were

Table 1b
New and published major element data for selected samples from the South Sandwich Arc, East Scotia Ridge, and the South American-Antarctic Ridge

	South Sandwich Island Arc (north to south)													
Location	Protector	Zavodovski	Zavodovski	Leskov	Leskov	Visikoi	Candlemas	Candlemas	Vindication	Vindication	Saunders	Montague	Bristol	Freezland
Sample no.	ssp1.1	ssz5.5	ssz83.4	ssl4.2	ssl12.1	ssw1.1	ss87.19	ss92.1	ssv2.1	ssv12.1	ss18.11	ss24.5	ss15.2	ssf2.11
Latitude (S)	55°45′	56°18′	56°18′	56°4′	56°4′	56°42′	57°05′	57°05′	57°1′	57°1′	57°45	58°25′	59°02′	59°02.5′
SiO_2	67.21	52.62	52.86	57.76	58.07	49.92	50.58	49.50	50.81	51.55	50.80	48.68	52.36	56.82
TiO_2	0.40	0.87	1.08	0.76	0.73	0.87	0.60	0.47	0.57	0.50	0.82	0.43	0.79	0.70
Al_2O_3	14.15	15.55	14.51	17.74	17.51	16.54	18.57	22.93	17.13	17.64	16.93	15.60	16.09	18.74
Fe_2O_3	4.11	12.31	13.62	7.23	7.39	11.41	10.15	7.34	10.07	9.55	10.43	9.79	11.96	7.75
FeO	–	–	–	–	–	–	–	–	–	–	–	–	–	–
MnO	0.10	0.22	0.25	0.14	0.16	0.17	0.18	0.12	0.19	0.18	0.17	0.17	0.20	0.15
MgO	0.99	6.22	5.04	3.86	3.82	6.65	6.60	4.10	6.12	6.83	7.38	10.87	5.41	2.53
CaO	4.44	10.37	9.66	7.98	7.91	11.71	11.67	13.35	13.27	12.27	11.40	13.38	10.37	8.24
Na_2O	5.22	1.47	2.68	3.20	2.93	1.88	1.83	1.57	1.70	1.73	2.16	1.22	2.41	3.38
K_2O	0.54	0.15	0.25	0.83	0.84	0.26	0.13	0.09	0.12	0.10	0.35	0.08	0.35	0.82
P_2O_5	0.08	0.05	0.07	0.13	0.12	0.08	0.04	0.05	0.04	0.01	0.10	0.03	0.10	0.13
LOI	2.96	–	–	–	0.29		−0.34	−0.11	–	–	−0.43	−0.37	−0.37	0.11
Total	100.20	99.83	100.02	99.63	99.77	99.49	100.01	99.41	100.02	100.36	100.12	99.88	99.69	99.37
Ref.	a	a	a	a	a	a	b		a	a				a

Note: there are no major element data available for sediments of Table 1a, nor samples WJ10b, ATL34.15 and v36.26 from Bouvet-SAAR. References are: (a) [4]; (b) [35]; (c) [28]; (d) [37]; (e) [39]; (f) [65].

Table 1b (*continued*)

	South Sandwich Island Arc (north to south)									East Scotia Ridge (north to south)					
Location	Freezland	Bellingshausen	S. Thule	Cook	Nelson Smt	Nelson Smt	Kemp Smt	Kemp Smt	Kemp Smt	E1	E1	E2	E2	E2	E2
Sample no.	ssf2.11	ss17.10	sst5.11	ss14.112	dr111.2	dr111.14c	dr112.6a	dr112.11a1	dr112.31	dr56.4	**dr60.1**	**wx3**	dr157.1	dr158.4	dr158.23
Latitude (S)	59°02.5′	59°26′	59°28′	59°28′	60°0′	60°0′	59°55′	59°55′	59°55′	55°32′	55°09′	56°6′	56°7′	56°7′	56°7′
SiO_2	56.82	56.55	55.67	52.64	65.15	64.97	50.83	53.06	49.96	51.40	50.88	53.45	49.98	53.61	55.26
TiO_2	0.70	0.93	1.10	0.60	0.65	0.65	0.51	0.69	0.64	0.72	0.71	1.82	1.63	1.01	1.82
Al_2O_3	18.74	15.19	14.68	19.50	14.48	14.93	17.70	16.28	16.18	16.07	17.36	14.80	15.32	16.71	15.38
Fe_2O_3	7.75	11.80	12.74	9.52	6.23	6.33	10.13	11.98	11.97	8.25	8.75	–	9.57	8.00	10.11
FeO	–	–	–	–	–	–	–	–	–	–	–	10.75	–	–	–
MnO	0.15	0.19	0.25	0.17	0.12	0.12	0.18	0.21	0.21	0.16	0.14	0.20	0.16	0.14	0.17
MgO	2.53	3.24	3.57	4.10	1.29	1.41	5.64	4.48	5.22	8.80	8.15	4.89	7.46	5.59	3.48
CaO	8.24	8.22	8.05	10.91	5.79	5.88	12.06	10.84	11.40	11.62	11.96	8.96	11.89	10.13	7.00
Na_2O	3.38	3.25	3.25	2.57	3.37	3.40	1.06	2.02	1.59	2.14	2.12	2.81	2.83	2.60	4.22
K_2O	0.82	0.53	0.73	0.28	1.27	1.26	0.31	0.29	0.24	0.31	0.12	0.72	0.68	1.05	0.74
P_2O_5	0.13	0.15	0.15	0.08	0.14	0.14	0.07	0.08	0.06	0.06	0.04	0.26	0.26	0.23	0.33
LOI	0.11	−0.53	–	−0.36	0.58	0.58	−0.13	0.24	0.03	0.34	0.08	–	0.19	0.94	1.27
Total	99.37	99.53	100.19	100.00	99.07	99.67	98.49	100.16	97.49	99.87	100.30	99.02	99.96	100.01	99.79
Ref.	a		a	b	c	c	c	c	c	c	c	d	d	d	d

(*continued on next page*)

Table 1b (*continued*)

	East Scotia Ridge (north to south)									Bouvet and SAAR (east to west)				
Location	E2	E3	E4	E5	E6	E7	E8	E9	E10	SAAR	SAAR	SAAR	SAAR	SAAR
Sample no.	wx5	**dr20.36**	wx47	**wx48**	**106 DS-1**	**110DS-3**	dr24.24	**wx69**	dr118.3	v18.2	v27.34	v31.18	v39.73	v42.10
Latitude (S)	56°8′	56°24′	57°2′	57°25′	57°49′	58°44′	59°28′	60°20′	60°35′	55°52′	56°53.7′	57°34.4′	58°39.1′	59°21.8′
SiO_2	55.28	50.07	50.88	49.83	49.79	50.66	53.13	51.33	53.43	49.42	50.42	50.98	49.69	50.84
TiO_2	2.05	1.28	1.48	1.33	1.66	1.97	0.94	1.58	1.65	0.05	1.78	1.64	1.44	1.96
Al_2O_3	15.72	16.72	16.26	15.30	14.84	14.52	17.68	15.67	15.55	15.46	15.86	15.34	16.91	15.67
Fe_2O_3	–	8.28	–	–	–	–	9.08	–	11.92	–	–	–	–	–
FeO	10.45	–	7.88	8.26	9.18	9.93	–	8.69	–	10.28	8.56	9.27	7.78	10.21
MnO	0.18	0.13	0.18	0.18	0.21	0.19	0.14	0.18	0.19	0.22	0.17	0.18	0.15	0.20
MgO	3.90	7.49	6.35	8.13	7.82	6.81	5.08	7.22	2.75	6.34	7.22	7.05	6.85	6.81
CaO	7.55	11.37	10.82	11.60	10.94	11.02	10.33	11.02	7.97	11.00	11.09	11.06	10.92	10.17
Na_2O	3.68	3.17	3.02	3.29	2.91	2.98	2.83	3.50	3.81	3.03	3.33	3.41	3.80	3.60
K_2O	0.48	0.32	0.59	0.10	0.10	0.27	0.39	0.37	0.46	0.54	0.71	0.29	0.46	0.24
P_2O_5	0.29	0.14	0.34	0.26	0.26	0.32	0.10	0.33	0.19	0.29	0.28	0.16	0.16	0.25
LOI	–	0.63	–	–	0.20	–	0.43	0.34	0.36	1.65	0.75	0.64	0.85	0.71
Total	99.58	99.60	97.80	98.46	97.90	98.67	100.11	100.24	98.28	100.28	100.17	100.02	99.01	100.66
Ref.	d				e	e		e	c	f	f	f	f	f

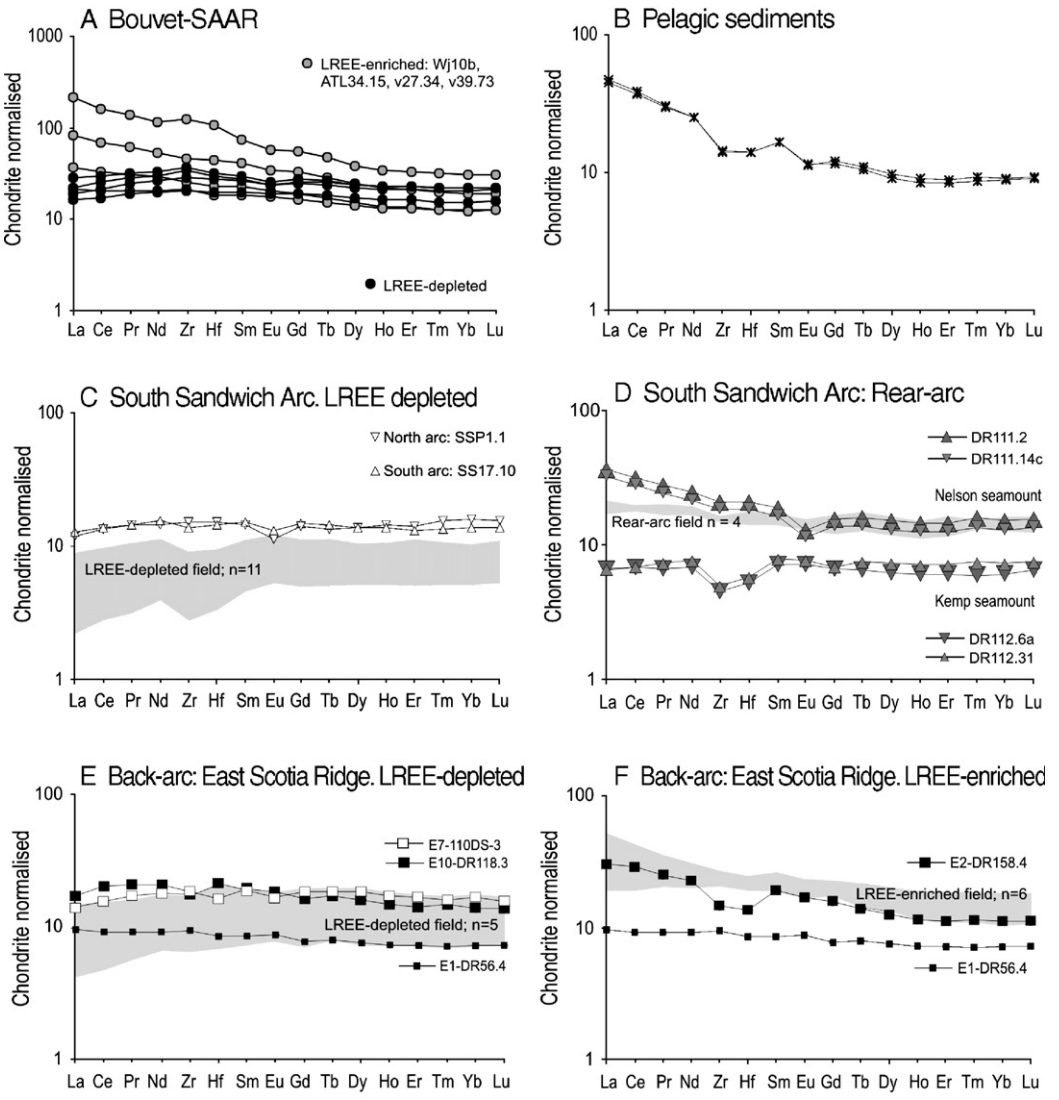

Fig. 2. Extended chondrite-normalized patterns for samples from (A) Bouvet-SAAR-ESR suite, (B) S. Atlantic sediments, (C) South Sandwich Island Arc (D) South Sandwich Island Rear-Arc, (E) Back-arc East Scotia Ridge—LREE-depleted, (F) Back-arc East Scotia Ridge—LREE-enriched. Chondrite normalization values from [49]. Note different *y*-axis scale for (A). Sample E1-DR.56.4 is plotted on both back-arc plots (E and F) for reference.

corrected for mass fractionation during the run by normalization to $^{179}Hf/^{177}Hf$ of 0.7325. Minimum uncertainties are derived from external precision of standard measurements for JMC 475 where JMC475 gave a value of 0.282116±0.000010 (2σ, n=14; P54 at NIGL) and 0.282154±0.000012 (2σ, n=9; Neptune at Frankfurt). To allow for inter-laboratory bias, results are quoted relative to a preferred value for JMC475 of 0.282160 [47]. After normalization, replicate analysis of our internal rock standard, pk-G-D12, over the period of analyses gave a result of 0.283050±0.000018 (2σ, n=11), comparable to previously reported values of 0.283049±0.000018 (2σ, n=27; [48]) and 0.283046±0.000016 (2σ, n=9; [47]).

4. Results

4.1. Hf and rare earth elements

In order to explore co-variation between Hf and REE we have characterized the groups of samples on the basis of their extended chondrite-normalized REE patterns (Fig. 2). For most processes involving partial melting of mantle and fractional crystallization of mafic magmas, Hf has a bulk distribution coefficient between that of Nd and Sm [49,50]. Chondrite-normalized plots for MORB and OIB with Hf plotted between Nd and Sm will therefore have a smooth pattern. However, if subduction-related processes cause

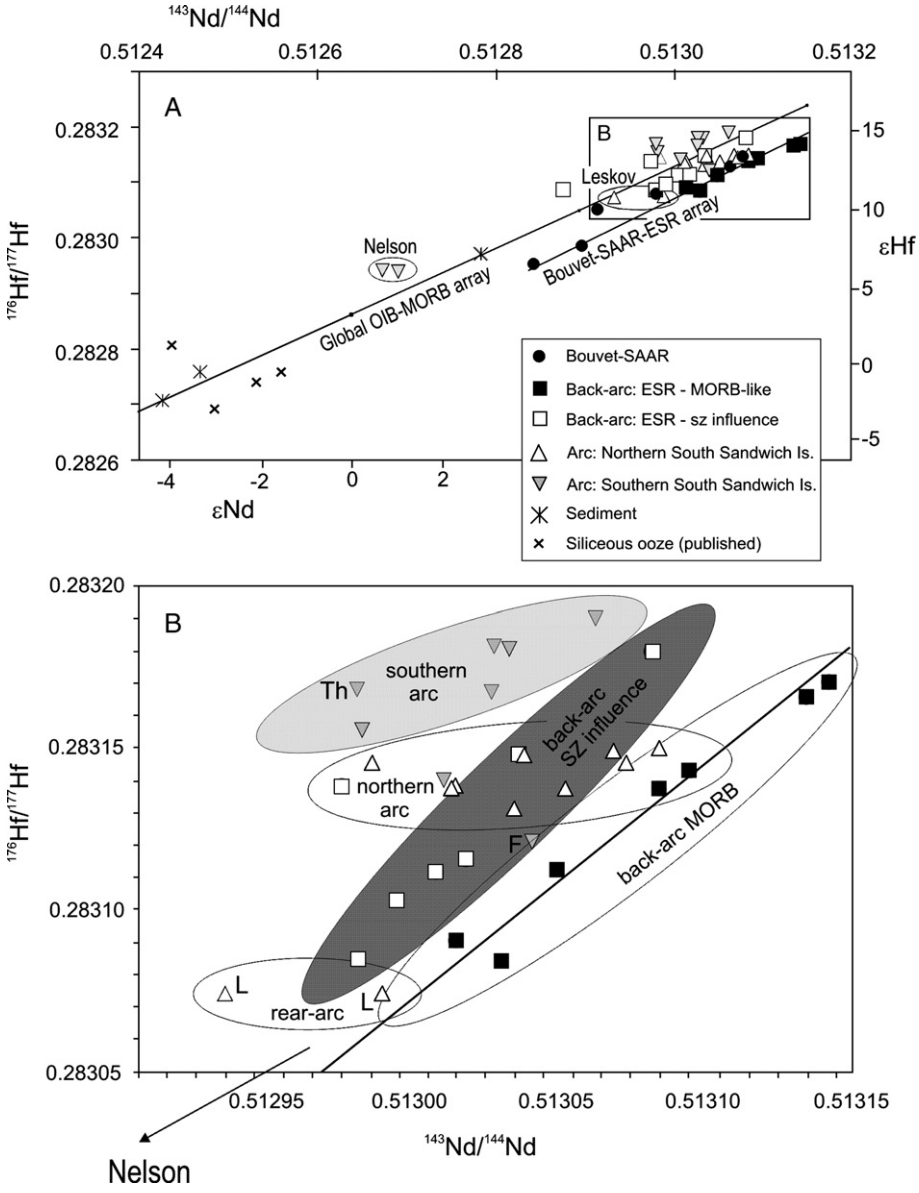

Fig. 3. (A) $^{176}Hf/^{177}Hf$ versus $^{143}Nd/^{144}Nd$ isotope diagram. Inset (B): enlarged area of Hf–Nd isotope plot showing detail of the majority of samples from the arc and back-arc.

decoupling of Hf from Nd then Hf anomalies will result (Fig. 2).

Samples from the Bouvet-SAAR-ESR suite fall into two groups: one group is made up of samples that are variably LREE-enriched; a second group is LREE-depleted (Fig. 2A). The LREE-enriched samples are not restricted to localities close to the Bouvet triple junction but include samples much further along the SAAR (see Fig. 1 for individual sample localities). As Fig. 2A shows, there is little variation in normalized Hf abundances relative to Nd and Sm in the LREE-depleted Bouvet-SAAR-ESR suite. The absence of Hf anomalies is an expected result of mantle melting in the absence of subduction processes.

The analysed pelagic sediments have virtually identical LREE-enriched patterns with pronounced negative Hf (and Zr) anomalies (Fig. 2B); such anomalies are likely caused by the preferential enrichment of REE due to adsorption onto clay minerals and sedimentary fractionation of zircon [51].

Most of the main arc samples (SSP1.1 and SS17.10 are exceptions) have LREE-depleted chondrite-normalized patterns and marked negative Hf anomalies (shaded field in Fig. 2C). A second group of samples from the arc has

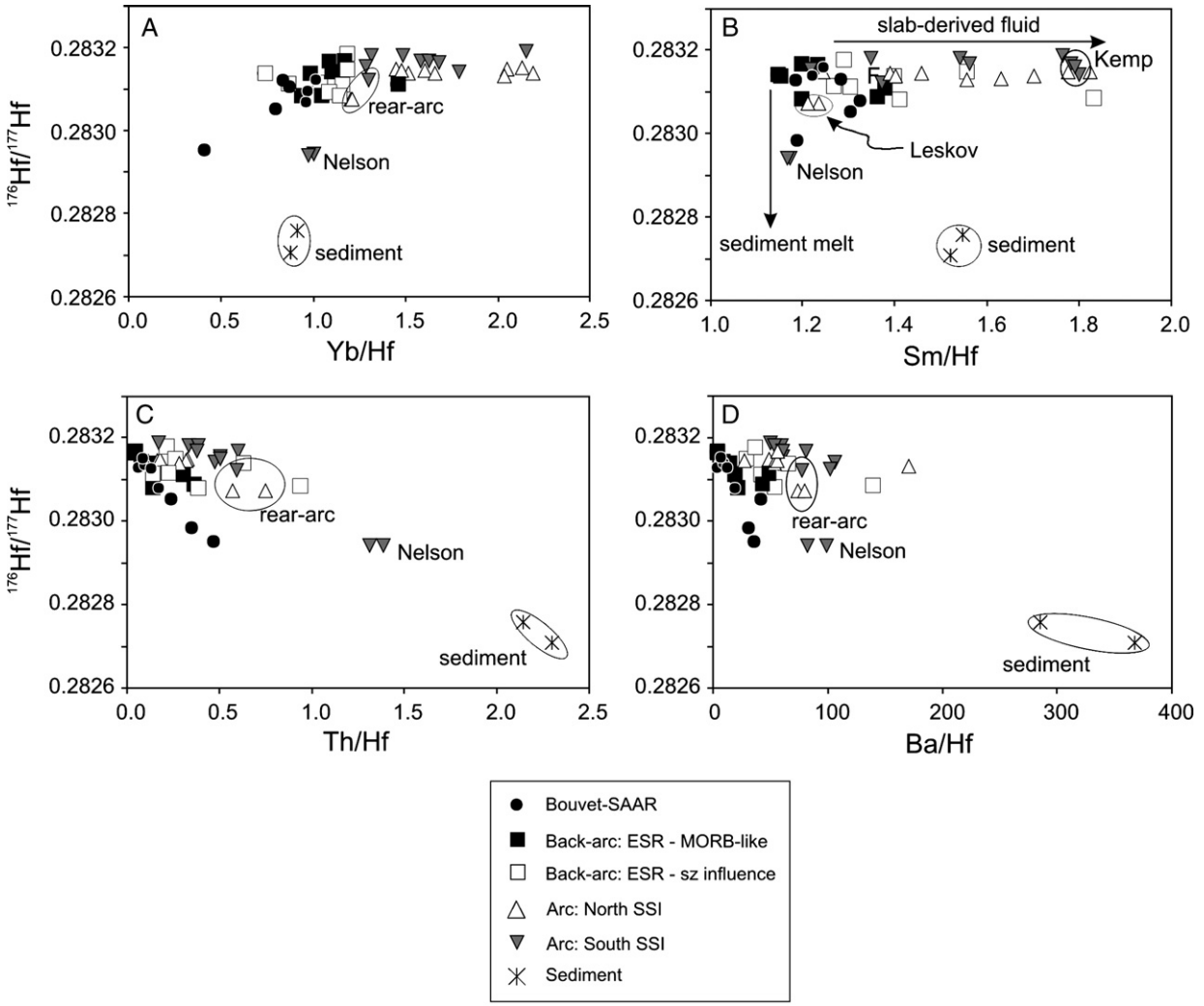

Fig. 4. $^{176}Hf/^{177}Hf$ versus trace element ratios: (A) Yb/Hf; (B) Sm/Hf, (C) Th/Hf, (D) Ba/Hf.

flat chondrite-normalized patterns with small negative Zr and Hf anomalies (shaded field in Fig. 2D); this second group consists of rear-arc samples SSL.14.2 and SS.12.1 (Leskov), as well as SSF.2.1 (Freezland) and SST.5.1 (Southern Thule) (Fig. 1, Tables 1a and b). Samples from Nelson and Kemp seamounts differ greatly from one another. Kemp, situated along the main arc trend, has a composition similar to other arc volcanoes: LREE-depleted normalized patterns and negative Hf anomalies. Nelson, in front of the main arc trend and in close proximity to the slab edge, has a normalized REE pattern akin to rear-arc samples but with greater LREE-enrichment (Fig. 2D).

The back-arc samples are variably LREE-depleted or -enriched (shaded fields in Fig. 2E and F, respectively) and overwhelmingly have small, slightly positive or slightly negative Hf anomalies. Three samples have larger Hf anomalies: samples DR.158.4 (E2) and 110DS-3 (E7) both have appreciable negative Hf anomalies (Fig. 2E and F), whereas DR.118.3 (E10) has a distinct positive anomaly (Fig. 2E).

Negative Hf and Zr anomalies, as seen in the arc samples and some back-arc samples, could result from two different processes. Firstly, addition of Nd and Sm but not Hf and Zr to the mantle wedge because Hf and Zr have much lower fluid/slab distribution coefficients. Alternatively, mixing of bulk sediment or a partial melt of sediment with the mantle wedge would impart negative Hf, Zr anomalies on the mantle wedge. Choosing between these alternatives is best done using Hf isotopes.

4.2. Hf–Nd isotopes

Using the eight selected samples from along the SAAR, we define a local OIB-MORB array within Hf–Nd isotopic

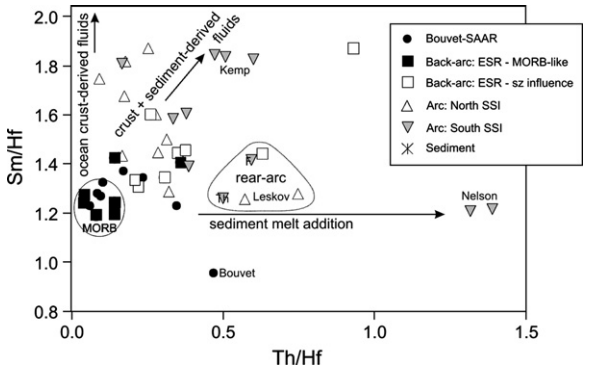

Fig. 5. Th/Hf versus Sm/Hf.

space (Fig. 3). This locally-defined Bouvet-SAAR-ESR array runs sub-parallel to the global array [52], but is offset towards lower Hf and/or higher Nd isotope ratios. This allows us to constrain the local background mantle composition from within an otherwise large global range. The local array is pinned at the OIB-end (lower $^{176}Hf/^{177}Hf$ and $^{143}Nd/^{144}Nd$ ratios) by the two samples closest to the Bouvet triple junction (WJ10b and ATL34.15). Both these samples are strongly LREE-enriched and lack an Hf anomaly (Fig. 2A). The MORB end of the array (higher $^{176}Hf/^{177}Hf$ and $^{143}Nd/^{144}Nd$ ratios) is pinned by the cluster of LREE-depleted samples v-18.2, -31.18, -36.26 and -42.10 (Figs. 2A and 3). Interestingly, two of the samples from the SAAR do not plot on our defined array (samples v-27.34 and v-39.73). These samples are mildly LREE-enriched (Fig. 2A) and have higher time-integrated Lu/Hf and/or lower time-integrated Sm/Nd than the other samples from along the spreading axis.

Seven ESR back-arc samples also plot along, or very close to, the defined Bouvet-SAAR-ESR array (sample numbers in bold in Tables 1a and b). These samples span ridge segments 1, 2, 3, 5, 6, 7 and 9 (Fig. 1) and have flat rare earth element chondrite-normalized patterns with slight depletion of LREE (Fig. 2E) indicating a MORB-like chemistry (exceptions to this are WX3 (E2) and WX69 (E9), which are subduction-modified [28]).

The low Hf isotope composition of the sediments agrees with values recorded on similar nearby sediments; four siliceous oozes from the SAAR have $^{176}Hf/^{177}Hf$ values between 0.282697 and 0.282805 [53] and between 0.512430 and 0.512553 [54].

4.3. Spatial distribution of Hf isotopes

It is evident from Fig. 3 that all the South Sandwich island arc samples are displaced from the local OIB-MORB array towards higher $^{176}Hf/^{177}Hf$ and/or lower $^{143}Nd/^{144}Nd$ ratios. A closer inspection of the arc data reveals a spatial distribution of Hf isotope ratios in which samples from the southern part of the arc (Montagu, and south; Fig. 1) have higher $^{176}Hf/^{177}Hf$ ratios than samples from the northern part of the arc (Fig. 3, inset). Exceptions to this are SSF2.1 from the southerly, rear-arc Freezland Island and two samples from the southerly Nelson seamount which all have low $^{176}Hf/^{177}Hf$ ratios (Fig. 3). A similar exception within the northern part of the arc is evident for rear-arc Leskov samples, SS14.2 and SSL12.1, which have markedly lower $^{176}Hf/^{177}Hf$ ratios than the remainder of the northern group.

These isotopic differences in samples from different parts of the South Sandwich arc are less obvious within the back-arc segment samples. The southern segments, E6 to E10, generally have higher $^{176}Hf/^{177}Hf$ than the northern segments, E1 to E5 (Tables 1a and b). However, as with the arc, there are exceptions: E9, which Leat et al. [28] shows to have a subduction component, has a lower $^{176}Hf/^{177}Hf$ ratio than other southerly segments; and the samples within E2, which also display a subduction component [28], have lower $^{176}Hf/^{177}Hf$ ratios than other northern segment samples. Thus, Hf isotope ratios within the back-arc samples correlate more with subduction influence than with location within the basin.

5. Discussion

Given the very low $^{176}Hf/^{177}Hf$ ratios of the local sediment, it is evident that the low $^{176}Hf/^{177}Hf$ values in arc samples from Nelson and Leskov, and some back-arc samples, can most easily be explained by incorporation of sediment within the source region. However, to investigate the validity of this conclusion, we examine plots of Hf isotope ratios versus elemental ratios M/Hf, where M is a trace element selected for its particular mobility or incompatibility with respect to Hf (Fig. 4). We have used Hf as the denominator, so that mixing trends are linear.

5.1. Hf isotope—element/Hf co-variations

Because radiogenic Hf is derived from the parental HREE, Lu, it is useful first to compare $^{176}Hf/^{177}Hf$ to an HREE. Fig. 4A plots $^{176}Hf/^{177}Hf$ against Yb/Hf. Samples from the Bouvet-SAAR-ESR array have a positive correlation in the diagram whereas most arc–back-arc samples lie along a horizontal trend. In detail, the arc–back-arc samples clearly fall into two tectonically-defined groups: the back-arc samples with generally low Yb/Hf (<1.2, excluding DR.60.1 with 1.46), and the arc samples with high Yb/Hf (>1.2) except for Nelson (Fig. 4A). Nelson, Leskov and, to a lesser degree, Freezland, have low Yb/Hf ratios and low $^{176}Hf/^{177}Hf$ ratios which

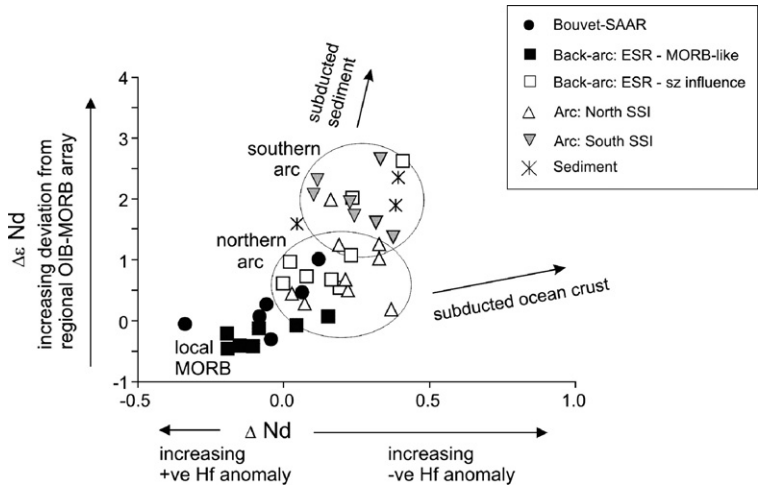

Fig. 6. ΔNd versus ΔεNd. Plot excludes data from Nelson and rear-arc samples Leskov and Freezland because they show Hf mobility. The arrows indicate vectors towards possible sources of fluid enrichment.

may, at face value, be explained by mixing with a component derived from unradiogenic sediment.

The positive correlation of Yb/Hf with $^{176}Hf/^{177}Hf$ in the OIB-MORB Bouvet-SAAR-ESR samples can be explained in terms of progressive melt extraction from a heterogeneous mantle [55]. The diagonal trend results when enriched 'plums' are preferentially extracted, so moving the isotope composition towards the depleted matrix and increasing the Yb/Hf ratio of the residual mantle asthenosphere. The flattening of the trend in the arc samples, i.e. increasing Yb/Hf ratios for fairly constant Hf isotope ratios, may be attributed to increasing source depletion as the mantle flows towards the arc front; the trend is flat because the enriched component has, by this stage, been removed. Supporting evidence for this interpretation comes from the good correlation between Zr/Yb and Nb/Ta in the arc samples, which all have subchondritic Nb/Ta (figure not shown; [35]). This is interpreted to be a result of prior melt extraction from the sub-arc source in the back-arc and arc, consistent with interpretations from other intra-oceanic arcs [10,56].

If we replace Yb with Sm, a middle-REE and the parent element of ^{143}Nd (Fig. 4B), we observe a wide range of Sm/Hf ratios which are not as tightly grouped into tectonic settings as Yb/Hf. High Sm/Hf values characterize samples from the northern volcanoes Zavadovski and Visikoi, as well as the southern seamount, Kemp. Sm and Hf have similar incompatibilities for mantle melting, so the effects of source depletion on Sm/Hf ratios will be low. However, Sm is thought to be more strongly mobilized in slab-derived fluids than Hf [4]. Therefore, we attribute the high Sm/Hf ratios to selective addition of Sm by aqueous fluids derived from the slab, though a similar result could be achieved by addition of Sm in lower temperature melts. As with Yb/Hf ratios, the rear-arc samples Nelson, Leskov and Freezland have lower Sm/Hf ratios than other arc samples, requiring Sm loss and/or Hf addition.

Thorium, a strongly incompatible large-ion-lithophile element (LILE), is generally abundant within subducted pelagic sediments, as well as being mobile in subduction settings. On a plot of $^{176}Hf/^{177}Hf$ versus Th/Hf, the majority of the arc samples have variable Th/Hf ratios up to 0.6, with little variation in Hf isotope ratios. This implies that much of the arc is dominated by the addition of fluids or melts that are unlikely to carry Hf but are relatively rich in Th. In contrast, Nelson seamount samples clearly plot toward the high Th/Hf ratios and low Hf isotope ratios of pelagic sediments (DR113.3 and -30). This vector requires addition of Hf as well as Th (Fig. 4C), and hence melt rather than fluid contribution from the slab. Furthermore, the displacement to low Hf isotope ratios indicates that the melt is sediment-derived. Conversely, Th addition without Hf addition, present throughout most of the arc, is most likely to be fluid-controlled, albeit in a high-*T* phase, in which only Th is mobile.

Finally, we use Ba, a LILE which, unlike Th, is easily mobilized by low temperature aqueous fluids [8] (Fig. 4D). The data fall into two groups, with little overlap: back-arc samples generally have low Ba/Hf (3.48 to 66.2, excluding subduction-modified E2 sample DR.158.4) and arc samples have higher Ba/Hf (27.7 to 170.2). It is not clear whether the Ba contribution to the arc is derived from sediment or from altered oceanic

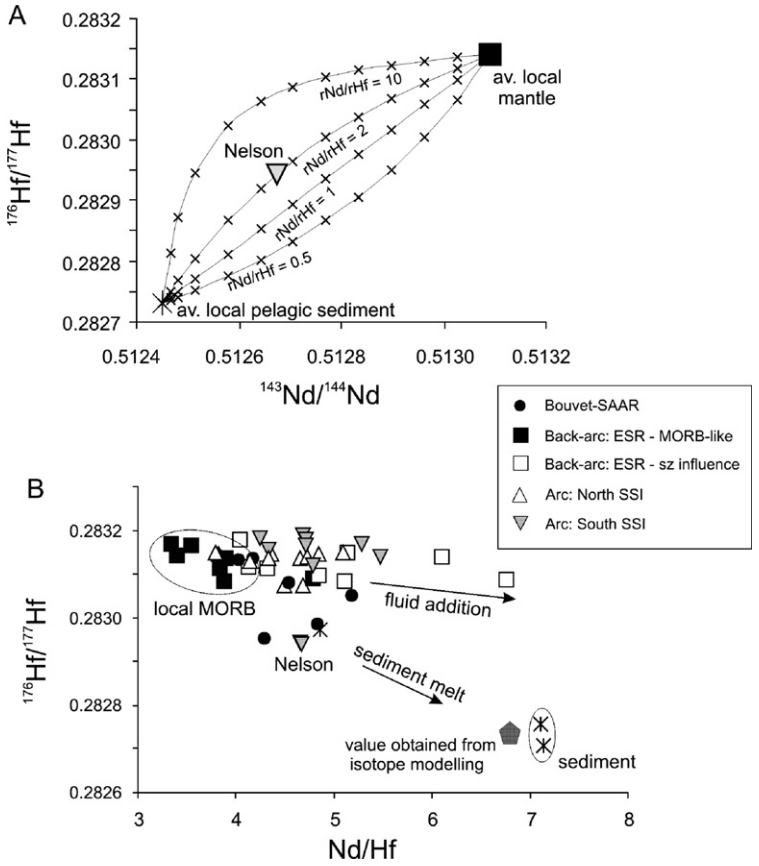

Fig. 7. (A) Modelled mixing curves on a plot of $^{176}Hf/^{177}Hf$ versus $^{143}Nd/^{144}Nd$. (B) $^{176}Hf/^{177}Hf$ versus Nd/Hf.

crust. However, based on the absence of correlation between $^{176}Hf/^{177}Hf$ ratios and Ba/Hf, we can infer that either (1) Ba is mobilized by low-*T* fluids during shallow slab dehydration while Hf is not mobile, or (2) Ba addition derives from material that isotopically is little different from the mantle wedge, i.e. from dehydration of altered oceanic crust.

5.2. Element/Hf (ppm) co-variations

To further examine the relative roles of fluid- versus melt-contribution to the arc magma source we plot Sm/Hf versus Th/Hf (Fig. 5). It is clear from Fig. 4B that most of the arc samples, excluding Nelson and those from rear-arc volcanoes, are influenced by Sm addition (high Sm/Hf) from slab-derived fluids. Therefore we identify one of three trends in Fig. 5 as trending towards high Sm/Hf at low and constant Th/Hf which may be explained by the addition of a low-*T* fluid that carried Sm but not Th or Hf. The trend of increasing Sm/Hf with increasing Th/Hf may be interpreted as addition of a high-*T* fluid which carried both Sm and Th, but not Hf (compare Figs. 4B and 5, especially for samples from Kemp). In contrast, Nelson and, to a lesser degree, the rear-arc volcanoes trend towards increasing Th/Hf at constant and low Sm/Hf. This may be interpreted as addition of a partial melt of sediment that carried Th and Hf, but relatively low Sm. Samples demonstrating addition of a sediment melt component are those close to a slab-edge and/or within a rear-arc setting (Fig. 5).

These inferences contrast with earlier work that recorded Th mobilization relative to, say, the behaviour of Ba. Because an all-pervading enrichment in Ba was assumed to represent a fluid phase [7,8], it followed that Th enrichment must represent a melt phase. Our results point towards Th mobilization not only in melts but also in a fluid phase, which we propose is most likely to be higher temperature than that which transports Ba and other highly incompatible elements.

5.3. Quantifying Hf addition to the mantle wedge

The Hf–Nd isotope plot provides evidence that an Hf-bearing sediment component contributes to Nelson seamount volcanism. From our detailed examination of plots of Hf isotopes versus trace element ratios, it is evident

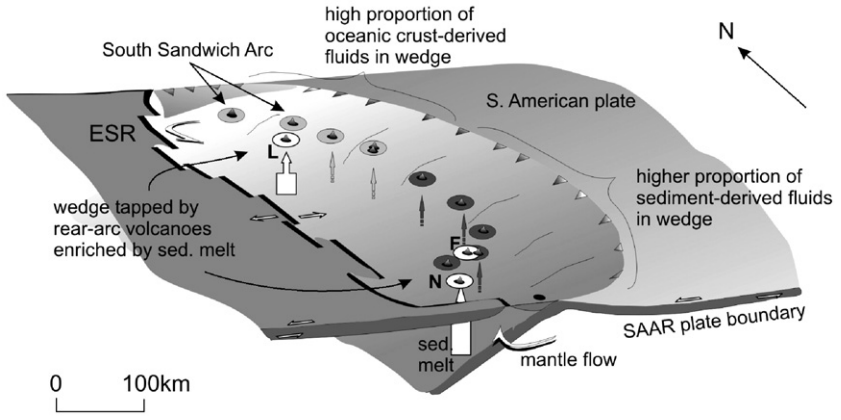

Fig. 8. 3-dimensional oblique cut-out view of the S. Sandwich Arc and inferred sources of enrichment to the wedge. L—Leskov; F—Freezland; N—Nelson. Thin dark arrows are inferred transfer of fluids from the slab. Thick light arrows are inferred transfer of sediment melt from the slab to the wedge. Note the difference in style of slab edges—a tear in the north versus a plate boundary in the south. Flow around the edge of the slab in the north is deflected to a greater depth than in the south due to downwarping of the S. American plate.

that samples from the rear-arc islands, Leskov, Freezland and possibly, though much less compelling, Southern Thule, also have markedly lower $^{176}Hf/^{177}Hf$ ratios than the other arc samples (Figs. 3–5). Although Nelson and the rear-arc samples have lower $^{176}Hf/^{177}Hf$ ratios than the other arc samples, they do not exhibit Hf anomalies on extended REE plots (Fig. 2). Conversely, it is interesting that the main arc samples, which do not have these lower $^{176}Hf/^{177}Hf$ ratios, have negative Hf anomalies (Fig. 2).

To further understand the behaviour of Hf during subduction and to constrain the addition of Hf to the mantle wedge source region, we must first define the local OIB-MORB array as illustrated in Fig. 3. The local array can be calculated as:

$$\varepsilon Nd = 0.717\varepsilon Hf - 0.565. \quad (1)$$

Calculation of deviation from the array (ΔεNd), parallel to the Nd axis, can therefore be expressed as:

$$\Delta\varepsilon Nd = 0.710\varepsilon Hf - 0.604 - \varepsilon Nd. \quad (2)$$

If Hf behaves conservatively and Nd non-conservatively during slab dehydration, then displacement from the OIB-MORB array, as defined by ΔεNd, should correlate with the amount of Nd, relative to Hf, added from the subduction zone, i.e. by the size of the negative Hf anomaly on an extended REE plot. The correlation will be linear if the size of the anomaly is expressed as ΔNd, where ΔNd is a function of the difference between the observed value (o) and the expected value (e) on the OIB-MORB array on a plot of Nd/Yb against Hf/Yb [23]:

$$\Delta Nd = \frac{\left(\frac{Nd}{Yb}\right)_o - \left(\frac{Nd}{Yb}\right)_e}{\left(\frac{Nd}{Yb}\right)_o} \quad (3)$$

With the expected value calculated from:

$$\log\left(\frac{Nd}{Yb}\right) = 1.341\log\left(\frac{Hf}{Yb}\right) + 0.617 \quad (4)$$

Fig. 6 is a plot of ΔεNd (the deviation from the regional mantle array as defined on an Hf–Nd isotope plot) against ΔNd (the deviation from the elemental array and thus the magnitude of any existing Hf anomaly). On this plot, we have drawn the expected trends for derivation of the added Nd from (1) subducted sediment (assumed from existing data set to approximate to εNd=−4); and (2) subducted oceanic crust (assumed to approximate to εNd=8). As previously discussed, Hf addition to the mantle beneath Nelson and the rear-arc samples is much greater than for other arc samples. Subsequently, rear-arc samples will have experienced smaller than predicted elemental displacements for any given isotopic shift. Therefore if we omit these samples from Fig. 6, we leave only those samples where Hf appears to behave conservatively. Fig. 6 shows the arc and back-arc data fanning out from the composition of the MORB-like basin samples which are unaffected by subduction. Two clusters are apparent:

1. The northern arc-islands (Zavodovski, Visikoi, Candlemas, Vindication and Saunders) overlap and have only a minor increase in ΔεNd from MORB samples. Neodymium addition is not accompanied by large shifts in the Nd isotope signature and may be interpreted as addition of Nd from a source with a similar isotopic composition to the mantle wedge, i.e. mainly oceanic crust. This projection shows that the relatively large negative Hf anomalies observed (Fig. 2) may be

achieved with only little change in the Nd isotope composition.

2. The southern islands (Montagu, Bristol, Cook, Kemp) have a steeper trend i.e. larger isotope shifts for a given Nd addition. This indicates that, relative to the northern arc-islands, these samples have large isotopic shifts for negative Hf anomalies. This can be interpreted as addition of Nd from a source significantly different isotopically from the mantle wedge, i.e. mainly pelagic sediment.

Thus, assessment of combined isotope and element shifts indicates a dominantly pelagic sediment input throughout the arc but a greater proportion of oceanic crustal component in the north. The apparent absence of Hf mobility, except for Nelson and the rear-arc volcanoes, indicates that both of these components are likely derived from a fluid or a low temperature melt rather than a high temperature (i.e. significantly suprasolidus) melt. Shifts in Hf isotope ratios (Fig. 3) are evidence that the component contributing to Nelson and Leskov, and less compelling but potentially to Freezland and Southern Thule also, is most likely a high temperature melt.

5.4. Investigating the composition of the source component for Nelson seamount

In order to assess whether Nelson seamount and the rear-arc volcanoes reflect a mantle wedge source enriched by slab-derived melts, as we predict, we model the Hf–Nd isotope data. The modelling places constraints on the relative mobilities of Nd and Hf, and uses a standard mixing equation (where f is the mass fraction of the subduction component and subscripts m, sz and w refer to the mantle component, subduction zone component, and mantle wedge respectively [23]):

$$\varepsilon Nd_w = \frac{\varepsilon Nd_m(1-f)\mathrm{Nd}_m + \varepsilon Nd_{sz} f \mathrm{Nd}_{sz}}{(1-f)\mathrm{Nd}_m + f\mathrm{Nd}_{sz}} \quad (5)$$

From Eq. (4) it is possible to define the ratio r_{Nd} as the mass fraction of Nd in the subduction zone component compared to the mass fraction in the mantle component. Because r equals Nd_{sz}/Nd_m, we can substitute Nd_{sz} for rNd_m in the equation, which then becomes [23]:

$$\varepsilon Nd_w = \frac{\varepsilon Nd_m(1-f) + r_{Nd} f \mathrm{Nd}_{sz}}{1-f(1-r_{Nd})} \quad (6)$$

To model the Nelson data, we assume an isotopic composition for a mantle end-member that shows no subduction component, estimated from East Scotia Ridge basalts (average of the E5, E6, E7 and E9 samples: $^{176}Hf/^{177}Hf = 0.28314$ and $^{143}Nd/^{144}Nd = 0.51309$). Furthermore, we assume a composition for subducted sediment from the average of the pelagic sediments ($^{176}Hf/^{177}Hf = 0.28273$ and $^{143}Nd/^{144}Nd = 0.51245$). Fig. 7A presents mixing curves for various ratios of r_{Nd}/r_{Hf} and demonstrates that the best fit is obtained with a ratio of about 2. Thus:

$$2.0 = \frac{\mathrm{Nd}_{sz}}{\mathrm{Nd}_m} \Big/ \frac{\mathrm{Hf}_{sz}}{\mathrm{Hf}_m} = \frac{\mathrm{Nd}_{sz}}{\mathrm{Hf}_{sz}} \Big/ \frac{\mathrm{Nd}_m}{\mathrm{Hf}_m} \quad (7)$$

The Nd/Hf ratio for average East Scotia Ridge MORB basalt is 3.54 (Tables 1a and b) which, taking into account slight fractionation during partial melting, converts to an Nd_m/Hf_m ratio of about 3.4 in the mantle source. Thus the Nd/Hf ratio in the subduction component equals $Nd_{sz}/Hf_{sz} = 3.4 \times 2.0 = 6.8$. This value is less than that obtained for the two pelagic sediments (7.11 and 7.14; Fig. 7B), indicating that, with regards to the subduction component added to the mantle wedge beneath Nelson seamount, Hf has been mobilized more readily than Nd. Evidence that Nelson reflects enrichment from a slab-derived pelagic sediment melt component, rather than a volcaniclastic component, is consistent with the mixing curves of Tollstrup and Gill ([57]; using local end-member compositions for mantle and pelagic sediments). Furthermore, Leskov and Freezland plot on the same mixing lines ([57], Fig. 3).

5.5. Interpreting the significance of a north–south compositional difference

Excluding Nelson and the rear-arc volcanoes, the northern main arc samples, Protector to Saunders, have lower $^{176}Hf/^{177}Hf$ ratios (0.283131 to 0.283150) than the southern volcanoes, Montagu to Kemp (0.283141 to 0.283190; Fig. 3). Interestingly, the north–south divide is coincident with a discontinuity on the opposing subducting S. American plate which, when extrapolated, would lie between Saunders and Montagu. Given the evidence from Fig. 4 that Hf has been effectively conservative beneath these arc volcanoes, we can rule out melt transfer from heterogeneous downgoing sediment. Thus, the systematic compositional variation must be independent of the slab conditions, and therefore originate within the mantle wedge. For example, the variation could be attributed to more OIB-like wedge material in the north compared to a more MORB-like composition in the south. Alternatively, it could reflect a longer history of subduction processes recorded in the northern mantle wedge than the south with an earlier phase of Hf mobility

that enriched the wedge with Hf-bearing melts. By way of comparison, the mantle wedge beneath the Izu-Bonin arc is also reported as having compositional zonation, with depleted mantle wedge found in the volcanic front versus fertile mantle wedge present beneath the back-arc [58].

5.6. Understanding conditions controlling fluid- versus melt-enrichment

As shown above, pelagic sediments have very low $^{176}Hf/^{177}Hf$ ratios and thus will impart a lower $^{176}Hf/^{177}Hf$ ratio upon a melt generated from mantle wedge enriched by a sediment melt or a supercritical liquid. It is perhaps surprising then, that more of the samples from the South Sandwich arc are not displaced towards lower $^{176}Hf/^{177}Hf$ ratios as are samples from Nelson and the rear-arc volcanoes. Recent Hf–Nd studies of the Aleutian-Kamchatka island arc chain have revealed that most of the arc is underlain by mantle wedge that was enriched by fluids, and not melts, though in the fluid is dominantly derived from an oceanic crust parental material [26,27]. It has been inferred that enrichment by slab-derived (adakitic) melts is restricted to northern Kamchatka and the western Aleutians [26,27].

The apparent lack of sediment melt contribution to most South Sandwich arc rocks could be the result of the predominantly siliceous composition of the sedimentary pile. Although it is true that pure siliceous ooze will have an average melting point higher than a more terrigenous sedimentary sequence or GLOSS [59], such oozes contain a significant proportion (up to 20% by weight) of non-siliceous components such as airborne particulates, hydrogenous minerals and volcanic ash. These would be sufficient enough, at a water-saturated solidus, to generate a melt that could explain the geochemistry of Nelson seamount. Melting temperatures need not differ greatly from those of clay-rich, but silica-poor, pelagic sediments studied experimentally [8,60]. Tables 1a and b shows that the S. Atlantic oozes have high concentrations of incompatible elements that, if melted, could be partitioned into early melt fractions. The absence of such a signature in most South Sandwich arc lavas suggests that, predominantly, temperatures are insufficient to cause melting.

An interesting similarity in the setting of the melt-enriched segments of the northern Kamchatka-Aleutian arc and Nelson seamount is their proximity to a slab edge [61]. This is likely to be an important factor in the cause of melt-dominated enrichment, though clearly cannot account for the enrichment evident within the South Sandwich rear-arc volcanoes. If melt production from slabs relates to high temperatures along the edges (e.g. 28), this Hf isotope study may indicate that the rear-arc setting was also fed by a subduction component derived from a high temperature slab, most obviously due to the greater depth of the slab beneath the arc. This is in agreement with seismic data from the NE Taiwan margin, where a low velocity lens has been imaged in the mantle, between 20 and 100 km depth, above a slab edge [62]. This low velocity lens has been attributed to an H_2O-rich and/or melt component and thought to result from either (1) additional release of H_2O along the vertical edge of the slab or (2) upwelling of hot mantle around the plate edge [62].

Laboratory experiments on the thermal evolution of mantle during slab rollback and down-dip subduction have produced contrasting results [63]. The experiments modelled higher temperatures at centres than at edges of slabs undergoing rollback, but greater heating along the slab edges during down-dip subduction. However, Leat et al. [28] proposed that, during slab rollback, incoming asthenospheric mantle caused increased melting at slab edges. A key factor is likely to be the temperature of the incoming mantle: there is no evidence that sediment melt contributed to magmas at the Protector seamount on the northern edge of the South Sandwich arc, perhaps because the mantle in the north is cooler than in the south, reflecting its greater distance from the SAAR.

5.7. Implications for long-term evolution of mantle wedge chemistry

An important question is what proportion of melt extracted from subducted sediment is returned to the crust via magmatic activity, and what proportion remains in the mantle wedge. The South Sandwich arc lacks a sedimentary accretionary prism, and the amount of sediment subducted is large compared to the few volcanoes influenced by melts derived from sediment. The South Sandwich island data indicate that if partial melting of the subducted sediment is at all widespread, most of the melt must remain within the mantle wedge. Because sediment melt in a subduction setting will have a lower Nd/Hf ratio than a bulk sediment melt (Fig. 7B), a distinct chemical signature will be imparted on the evolution of that mantle wedge material. The wedge lithosphere or recycled asthenosphere will develop low Nd/Hf, and higher Lu/Hf than Sm/Nd ratios that, over time, would evolve into high $^{176}Hf/^{177}Hf$ isotope ratios compared to $^{143}Nd/^{144}Nd$. This type of process has been proposed to explain the composition of Indian Ocean ridge basalts where $^{176}Hf/^{177}Hf$ ratios are displaced above the global OIB-MORB array towards values of <0.283141 [48].

6. Conclusions

In order to explain the lack of Hf enrichment in arc magmas, it is usual to assume that Hf, like other HFSE, remains in the slab during subduction processes. However, this study shows that Hf can be mobilized from the slab, though only during high-*T* slab (sediment and/or ocean crust) melting. In the South Sandwich arc, the conditions under which such mantle wedge enrichment is sampled by arc magmas is restricted to rear-arc locations and proximity to a slab edge, which in turn is dependent upon the mantle flow pattern, the temperature of incoming mantle, and the depth of melting (Fig. 8). Under these conditions, we find that very little sediment is recycled to the arc as melt, and that most of the arc volcanoes demonstrate only aqueous fluid-derived/low-*T* melt mantle wedge enrichment. A sediment melt component can be recognized in Nelson seamount, near the southern slab edge of the South Sandwich arc and in rear-arc samples from Leskov and Freezland. We conclude that this is possible because the southern slab edge is adjacent to the SAAR and hence high temperature asthenosphere and because of the greater depth to the slab beneath the rear-arc volcanoes. ΔεNd values indicate that the sources of both northern and southern arc volcanoes experienced fluid addition from subducted sediment, although the source of the northern arc volcanoes was modified by a slightly higher proportion of crust-derived fluids. The Hf isotope data, supported by the absence of adakites or boninites, do not support melting of oceanic crust in the South Sandwich arc-basin system.

Acknowledgements

This work has been funded by the NERC Antarctic Funding Initiative Grant Number AFI-12/36. The authors would like to thank S. Fretzdorff for the East Scotia Ridge WX samples. A. Gerdes is thanked for assistance with Hf analyses in Frankfurt. We thank J. Gill and J. Patchett for their helpful comments on the manuscript.

Appendix 1

	JB-1a (average, $n=5$)	JB-1a (recommended [64])
Sc	28.3	27.9
V	186.9	205
Cr	481	392
Co	37.8	38.6
Ni	136	139
Cu	54.1	56.7
Ga	18.0	17.0

Appendix 1 (*continued*)

	JB-1a (average, $n=5$)	JB-1a (recommended [64])
Rb	38.6	39.2
Sr	453	442
Y	23.7	24.0
Zr	140.7	144.0
Nb	27.9	26.9
Cs	1.20	1.31
Ba	496	504
La	38.9	37.6
Ce	67.1	65.9
Pr	7.3	7.3
Nd	26.8	26.0
Sm	5.08	5.07
Eu	1.51	1.46
Gd	4.96	4.67
Tb	0.72	0.69
Dy	4.02	3.99
Ho	0.79	0.71
Er	2.19	2.18
Tm	0.33	0.33
Yb	2.1	2.1
Lu	0.32	0.33
Hf	3.53	3.41
Ta	1.73	1.93
Pb	7.35	6.76
Th	8.21	9.03
U	1.59	1.57

Values quoted in ppm [63].

References

[1] M.R. Perfit, D.A. Gust, A.E. Bence, R.J. Arculus, S.R. Taylor, Chemical characteristics of island-arc basalts: implications for mantle sources, Chem. Geol. 30 (1980) 227–256.
[2] Y. Tatsumi, S. Eggins, Subduction Zone Magmatism, Blackwell Science, Cambridge, MA, 1995, 211pp.
[3] J.A. Pearce, D.W. Peate, Tectonic implications of the composition of volcanic arc magmas, Annu. Rev. Earth Planet. Sci. 23 (1995) 251–285.
[4] J.A. Pearce, P.E. Baker, P.E. Harvey, I.W. Luff, Geochemical evidence for subduction fluxes, mantle melting and fractional crystallization beneath the South Sandwich Island Arc, J. Petrol. 36 (1995) 1073–1109.
[5] C.J. Hawkesworth, K. Gallagher, J.M. Hergt, F. McDermott, Mantle and slab contributions in arc magmas, Annu. Rev. Earth Planet. Sci. 21 (1993) 175–204.
[6] C.J. Hawkesworth, S.P. Turner, F. McDermott, D.W. Peate, P. van Calsteren, U–Th isotopes in arc magmas: implications for element transfer from the subducted crust, Science 276 (1997) 551–555.
[7] T. Elliott, T. Plank, A. Zindler, W.M. White, B. Bourdon, Element transport from slab to volcanic front at the Mariana arc, J. Geophys. Res. 102 (1997) 14991–15019.
[8] M.C. Johnson, T. Plank, Dehydration and melting experiments constrain the fate of subducted sediments, Geochem. Geophys. Geosyst. 1 (1999) (1999GC000014).
[9] S.P. Turner, C.J. Hawkesworth, Constraints on flux rates and mantle dynamics beneath island arcs from Tonga-Kermadec lava geochemistry, Nature 389 (1997) 568–573.

[10] D.W. Peate, J.A. Pearce, Causes of spatial compositional variations in Mariana arc lavas: trace element evidence, Isl. Arc 7 (1998) 479–495.
[11] J.D. Woodhead, S.M. Eggins, R.W. Johnson, Magma genesis in the New Britain island arc: further insights into melting and mass transfer processes, J. Petrol. 39 (1998) 1641–1668.
[12] C. Class, D.M. Miller, S.L. Goldstein, C.H. Langmuir, Distinguishing melt and fluid subduction components in Umnak volcanics, Aleutian arc, Geochem. Geophys. Geosyst. 1 (2000) (1999GC000010).
[13] J.B. Gill, Orogenic Andesites and Plate Tectonics, Springer-Verlag, Berlin, 1981.
[14] J.G. Ryan, J.D. Morris, F. Tera, W.P. Leeman, A. Tsvetkov, Cross-arc geochemical variations in the Kurile arc as a function of slab depth, Science 270 (1995) 625–627.
[15] J.M. Brenan, H.F. Shaw, F.J. Ryerson, D.L. Phinney, Mineral-aqueous fluid partitioning of trace elements at 900 °C and 2.0 GPa—constraints on the trace element chemistry of mantle and deep crustal fluids, Geochim. Cosmochim. Acta 59 (1995) 3331–3350.
[16] J.M. Brenan, F.J. Ryerson, H.F. Shaw, The role of aqueous fluids in the slab-to-mantle transfer of boron, beryllium and lithium during subduction: experiments and models, Geochim. Cosmochim. Acta 62 (1998) 3337–3347.
[17] H. Keppler, Constraints from partitioning experiments on the composition of subduction zone fluids, Nature 380 (1996) 237–240.
[18] S.M. Peacock, Numerical-simulation of subduction zone pressure temperature time paths—constraints on fluid production and arc magmatism, Philos. Trans. R. Soc. Lond., A 335 (1991) 341–353.
[19] H. Bureau, H. Keppler, Complete miscibility between silicate melts and hydrous fluids in the upper mantle: experimental evidence and geochemical implications, Earth Planet. Sci. Lett. 165 (1999) 187–196.
[20] T. Moriguti, E. Nakamura, Across-arc variation of Li isotopes in lavas and implications for crust/mantle recycling at subduction zones, Earth Planet. Sci. Lett. 163 (1998) 167–174.
[21] T. Elliott, A. Jeffcoate, C. Bouman, The terrestrial Li isotope cycle: light-weight constraints on mantle convection, Earth Planet. Sci. Lett. 220 (2004) 231–245.
[22] W.M. White, J. Patchett, Hf–Nd–Sr isotopes and incompatible element abundances in island arcs: implications for magma origins and crust–mantle evolution, Earth Planet. Sci. Lett. 67 (1984) 167–185.
[23] J.A. Pearce, P.D. Kempton, G.M. Nowell, S.R. Noble, Hf–Nd element and isotope perspective on the nature and provenance of mantle and subduction components in western Pacific arc-basin systems, J. Petrol. 40 (1999) 1579–1611.
[24] J.D. Woodhead, J.M. Hergt, J.P. Davidson, S.M. Eggins, Hafnium isotope evidence for 'conservative' element mobility during subduction zone processes, Earth Planet. Sci. Lett. 192 (2001) 331–346.
[25] M. Bizimis, V.J.M. Salters, E. Bonatti, Trace and REE content of clinopyroxenes from supra-subduction zone peridotites. Implications for melting and enrichment processes in island arcs, Chem. Geol. 165 (2000) 67–85.
[26] B.R. Jicha, B.S. Singer, J.G. Brophy, J.H. Fournelle, C.M. Johnson, B.L. Beard, T.J. Lapen, N.J. Mahlen, Variable impact of the subducted slab on Aleutian Island arc magma sources: evidence from Sr, Nd, Pb, and Hf isotopes and trace element abundances, J. Petrol. 45 (2004) 1845–1875.
[27] C. Munker, G. Worner, G. Yogodzhinski, T. Churikova, Behaviour of high field strength elements in subduction zones: constraints from Kamchatka-Aleutian arc lavas, Earth Planet. Sci. Lett. 224 (2004) 275–293.
[28] P.T. Leat, J.A. Pearce, P.F. Barker, I.L. Millar, T.L. Barry, R.D. Larter, Magma genesis and mantle flow at a subducting slab edge: the South Sandwich arc-basin system, Earth Planet. Sci. Lett. 227 (2004) 17–35.
[29] P.F. Barker, I.A. Hill, Back-arc extension in the Scotia Sea, Philos. Trans. R. Soc. Lond., A A300 (1981) 249–262.
[30] R.D. Larter, L.E. Vanneste, P. Morris, D.K. Smythe, Tectonic evolution and structure of the South Sandwich arc, in: R.D. Larter, P.T. Leat (Eds.), Intra-oceanic subduction systems: Tectonic and Magmatic Processes, Spec. Publ.-Geol. Soc. Lond., vol. 219, 2003, pp. 255–284.
[31] C. Thomas, R. Livermore, F. Pollitz, Motion of the Scotia plates, Geophys. J. Int. 155 (2003) 789–804.
[32] P.F. Barker, Tectonic framework of the East Scotia Sea, in: B. Taylor (Ed.), Backarc Basins: Tectonics and Magmatism, Plenum Press, New York, 1995, pp. 281–314.
[33] L. Vanneste, R.D. Larter, Sediment subduction, subduction erosion and strain regime in the northern South Sandwich forearc, J. Geophys. Res. 107 (2002) 2149, doi:10.1029/2001JB000396.
[34] D.W. Forsyth, Fault plane solutions and tectonics of the South Atlantic and Scotia Sea, J. Geophys. Res. 80 (1975) 1429–1443.
[35] P.T. Leat, J.L. Smellie, I.L. Millar, R.D. Larter, Magmatism in the South Sandwich Arc, in: R.D. Larter, P.T. Leat (Eds.), Intra-oceanic subduction systems: Tectonic and Magmatic Processes, Spec. Publ.-Geol. Soc. Lond., vol. 219, 2003, pp. 285–313.
[36] R. Livermore, A. Cunningham, L.E. Vanneste, R.D. Larter, Subduction influence on magma supply at the East Scotia Ridge, Earth Planet. Sci. Lett. 150 (1997) 261–275.
[37] P.T. Leat, R.A. Livermore, I.L. Millar, J.A. Pearce, Magma supply in back-arc spreading centre segment E2, East Scotia Ridge, J. Petrol. 41 (2000) 845–866.
[38] N.J. Bruguier, R.A. Livermore, Enhanced magma supply at the southern East Scotia ridge: evidence for mantle flow around the subducting slab? Earth Planet. Sci. Lett. 191 (2001) 129–144.
[39] S. Fretzdorff, R.A. Livermore, C.W. Devey, P.T. Leat, P. Stoffers, Petrogenesis of the back-arc East Scotia Ridge, South Atlantic Ocean, J. Petrol. 43 (2002) 1435–1467.
[40] I.W. Hamilton, Geophysical investigations of subduction-related processes in the Scotia Sea. PhD thesis, Univ. Birmingham (1989).
[41] J.A. Pearce, P.T. Leat, P.F. Barker, I.L. Millar, Geochemical tracing of Pacific-to-Atlantic upper-mantle flow through the Drake Passage, Nature 410 (2001) 457–461.
[42] P.D. Kempton, Common Pb chemical procedures for silicate rocks and minerals, methods of data correction and an assessment of data quality at the NERC Isotope Geosciences Laboratory, NIGL Report Series 78 (1995) 26.
[43] K.R. Royse, P.D. Kempton, D.P.F. Darbyshire, Procedure for the analysis of rubidium–strontium and samarium–neodymium isotopes at the NERC Isotope Geosciences Laboratory, NIGL Report Series 121 (1998) 28.
[44] M.F. Thirlwall, Multicollector ICP-MS analysis of Pb isotopes using a ^{207}Pb–^{204}Pb double spike demonstrates up to 400 ppm/amu systematic errors in Tl-normalization, Chem. Geol. 184 (2002) 255–279.
[45] W. Todt, R.A. Cliff, A. Hanser, A.W. Hofmann, Evaluation of a ^{202}Pb–^{205}Pb double spike for high precision lead isotope analysis, in: S.R. Hart, A. Basu (Eds.), Earth Processes: reading

the isotope code, Geophys. Monogr. Ser., vol. 95, AGU, Washington, D.C., 1996, pp. 429–437.
[46] P.D. Kempton, G.M. Nowell, T.L. Barry, Procedure for the high precision isotopic analysis of hafnium in silicate rocks and minerals by plasma ionisation multi-collector mass spectrometry (PIMMS) and an assessment of data quality at the NERC Isotope Geosciences Laboratory, NIGL Report Series 171 (2001) 43.
[47] G.M. Nowell, P.D. Kempton, S.R. Noble, J.G. Fitton, A.D. Saunders, J.J. Mahoney, R.N. Taylor, High precision Hf isotope measurements of MORB and OIB by thermal ionisation mass spectrometry: insights into the depleted mantle, Chem. Geol. 149 (1998) 211–233.
[48] P.D. Kempton, J.A. Pearce, T.L. Barry, J.G. Fitton, C. Langmuir, D.M. Christie, Sr–Nd–Pb–Hf isotope results from ODP Leg 187: evidence for mantle dynamics of the Australian-Antarctic discordance and origin of the Indian MORB source, Geochem. Geophys. Geosyst. 3 (2002).
[49] S.-S. Sun, W.F. McDonough, Chemical and isotope systematics of oceanic basalts: implications for mantle composition and processes, in: A.D. Saunders, M.J. Norry (Eds.), Magmatism in the Ocean Basins, Spec. Publ.-Geol. Soc. Lond., vol. 42, 1989, pp. 313–345.
[50] T.H. Green, Experimental studies of trace-element partitioning applicable to igneous petrogenesis—Sedona 16 years later, Chem. Geol. 117 (1994) 1–36.
[51] P.J. Patchett, W.M. White, H. Feldmann, S. Kielinczuk, A.W. Hofmann, Hafnium/rare earth element fractionation in the sedimentary system and crustal recycling into the Earth's mantle, Earth Planet. Sci. Lett. 69 (1984) 365–378.
[52] J.D. Vervoort, P.J. Patchett, J. Blichert-Toft, F. Albarede, Relationships between Lu–Hf and Sm–Nd isotopic systems in the global sedimentary system, Earth Planet. Sci. Lett. 168 (1999) 79–99.
[53] W.M. White, J. Patchett, D. BenOthman, Hf isotope ratios of marine sediments and Mn nodules: evidence for a mantle source of Hf in seawater, Earth Planet. Sci. Lett. 79 (1986) 46–54.
[54] D. BenOthman, W.M. White, J. Patchett, The geochemistry of marine sediments, island arc magma genesis, and crust–mantle recycling, Earth Planet. Sci. Lett. 94 (1989) 1–21.
[55] J.A. Pearce, Geochemical Mantle preconditioning by melt extraction during flow: theory and petrogenetic implications, J. Petrol. 46 (2005) 973–997.
[56] S.M. Eggins, J.D. Woodhead, L.P.J. Kinsley, G.E. Mortimer, P. Sylvester, M.T. McCulloch, J.M. Hergt, M.R. Handler, A simple method for the precise determination of ≥40 trace elements in geological samples by ICPMS using enriched isotope international standardisation, Chem. Geol. 134 (1997) 311–326.
[57] D.L. Tollstrup, J.B. Gill, Hafnium systematics of the Mariana arc: evidence for sediment melt and residual phases, Geology 33 (2005) 737–740.
[58] A. Hochstaedter, J. Gill, R. Peters, P. Broughton, P. Holden, B. Taylor, Across-arc geochemical trends in the Izu-Bonin arc: contributions from the subducting slab, Geochem. Geophys. Geosyst. 2 (2001) (2000GC000105).
[59] T. Plank, C.H. Langmuir, The chemical composition of subducting sediment and its consequences for the crust and mantle, Chem. Geol. 145 (1998) 325–394.
[60] G.T. Nichols, P.J. Wyllie, C.R. Stern, Subduction zone melting of pelagic sediments constrained by melting experiments, Nature 371 (1994) 785–788.
[61] G.M. Yogodzinski, J.M. Lees, T.G. Churikova, F. Dorendorf, G. Woerner, O.N. Volynets, Geochemical evidence for the melting of subducting oceanic lithosphere at plate edges, Nature 409 (2001) 500–505.
[62] J.-Y. Lin, S.-K. Hsu, J.-C. Sibuet, Melting features along the western Ryukyu slab edge (northeast Taiwan): tomographic evidence, J. Geophys. Res. 109 (2004) B12402, doi:10.1029/2004JB003260.
[63] C. Kincaid, R.W. Griffiths, Laboratory models of the thermal evolution of the mantle during rollback subduction, Nature 425 (2003) 58–62.
[64] N. Imai, S. Terashima, S. Itoh, A. Ando, 1994 Compilation of analytical data for minor and trace elements in seventeen GSJ geochemical reference samples, 'Igneous Rock Series', Geostand. Newsl. 19 (1995) 135–213.
[65] A.P. le Roex, H.J.B Dick, A.M. Reid, F.A. Frey, A.J. Erlank, S.R. Hart, Petrology and geochemistry of basalts from the American-Antarctic Ridge, Southern Ocean: implications for the westward influence of the Bouvet mantle plume, Contrib. Mineral. Petrol. 90 (198), 367–380.